



**WARSAW UNIVERSITY  
OF TECHNOLOGY**

**FACULTY OF GEODESY  
AND CARTOGRAPHY**

Dr.-Ing. Ryszard Preuss



**LEIBNIZ UNIVERSITÄT HANNOVER**

**INSTITUTE OF PHOTOGRAMMETRY  
AND GEOINFORMATION**

Dr.-Ing. Karsten Jacobsen

Diploma thesis

# **Automatic Building Extraction from UltraCamD Images**

**Marcin Matusiak**

Hannover 2007

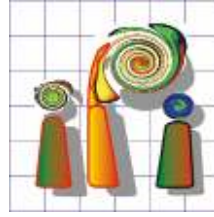




**WARSAW UNIVERSITY  
OF TECHNOLOGY**

**FACULTY OF GEODESY  
AND CARTOGRAPHY**

Dr.-Ing. Ryszard Preuss



**LEIBNIZ UNIVERSITÄT HANNOVER**

**INSTITUTE OF PHOTOGRAMMETRY  
AND GEOINFORMATION**

Dr.-Ing. Karsten Jacobsen

Diploma thesis

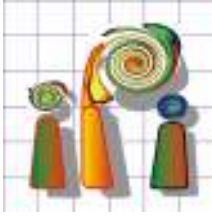
# **Automatic Buildings Extraction from UltraCamD Images**

**Marcin Matusiak**

Hannover 2007

I hereby assure that the present work was written independently  
and I have not used others than the stated sources and aids.

Marcin Matusiak  
Hannover, 10th of July 2007



**Institut für *P*hotogrammetrie und Geo*I*nformation**  
**Leibniz Universität Hannover**  
**Prof. Dr.-Ing. Christian Heipke**

Nienburger Str. 1  
D-30167 Hannover

Tel.: ++49-511/762-2485  
Fax: ++49-511/762-2483  
e-mail: [jacobsen@ipi.uni-hannover.de](mailto:jacobsen@ipi.uni-hannover.de)  
<http://www.ipi.uni-hannover.de>

**Dr.-Ing. Karsten Jacobsen**

---

Hannover, April 2007

## Automatic Building Extraction from UltraCamD Images

for Marcin Matusiak

The importance of 3D-city models is growing very fast. In relation to a two-dimensional GIS-representation the correct and detailed data acquisition for 3D-representation is very time consuming, raising the demand for automation. Different possibilities of automatic generation of digital surface models like airborne laser scanning and automatic image matching are available, but they have the disadvantage for not detailed and precise determination of the building edges.

Mr. Marcin Matusiak shall analyse the possibility of the generation of digital surface models by means of high resolution UltraCamD-images of 2 test areas in the city of Wroclav. Based on the digital surface models supported by building outlines from external data sources 3D-building models shall be generated and analyzed.

(Dr. Karsten Jacobsen)

## Table of contents

<b>1. INTRODUCTION .....</b>	<b>7</b>
1.1. OBJECTIVE OF WORK.....	7
1.2. SCOPE OF WORK.....	7
1.3. MOTIVATION .....	7
<b>2. THEORETICAL SECTION .....</b>	<b>9</b>
2.1. THREE DIMENSIONAL CITY MODELS.....	9
2.1.1. <i>Data sources</i> .....	9
2.1.2. <i>Applications</i> .....	12
2.1.3. <i>Generalization, Level of Details (LoD)</i> .....	14
2.2. AUTOMATIC IMAGE MATCHING .....	18
2.2.1. <i>Area Based Matching (ABM)</i> .....	19
2.2.2. <i>Feature Based Matching (FBM)</i> .....	22
2.3. AUTOMATIC EXTRACTION .....	25
2.3.1. <i>Model based methods</i> .....	25
2.3.2. <i>Data based methods</i> .....	28
<b>3. EXPERIMENTAL SECTION.....</b>	<b>32</b>
3.1. TEST AREA.....	32
3.2. STRATEGY .....	34
3.2.1. <i>Image matching – DPLX / DPCOR</i> .....	35
3.2.2. <i>Computation of a ground coordinates – BLPRE → BLINT</i> .....	43
3.2.3. <i>DSM analysis – DEMANAL</i> .....	43
3.2.4. <i>DSM interpolation and visualization – SURFER</i> .....	44
3.2.5. <i>DSM refinement – RASCOR</i> .....	47
3.2.6. <i>Building reconstruction – ATOP</i> .....	47
3.3. RESULTS .....	51
3.3.1. <i>Generation of DSM</i> .....	51
3.3.2. <i>Building reconstruction</i> .....	58
<b>4. CONCLUSION .....</b>	<b>63</b>
<b>ACKNOWLEDGEMENTS .....</b>	<b>65</b>
<b>APPENDIX.....</b>	<b>66</b>
<b>REFERENCES .....</b>	<b>77</b>

## List of figures

FIG 1.	DATA SOURCES .....	9
FIG 2.	POTENTIAL APPLICATIONS OF 3D CITY MODELS [SCHULZE-HORSEL, 2007].....	13
FIG 3.	SAMPLE GENERALIZATION OF THE BUILDING'S EDGES [KADA, 2003].....	14
FIG 4.	STAGES OF GENERALIZATIONS DEPENDING UPON DISTANCE OF THE OBSERVER .....	15
FIG 5.	LEVEL OF DETAILS ACCORDING TO CITYGML .....	17
FIG 6.	AERIAL IMAGE AND CORRESPONDING IMAGE FEATURES [FOERSTNER, 1999].....	23
FIG 7.	CSG RECONSTRUCTION TREE.....	25
FIG 8.	PARAMETRIC DESCRIPTION OF THE PRIMITIVES [SUVEG AND VOSELMAN, 2004] .....	25
FIG 9.	TERMINALS (LEFT) AND CONNECTORS (RIGHT); PLUG FACES, WHICH ARE USED TO CONNECT THEM, ARE DRAWN DASHED. [FISCHER ET AL., 1998] .....	27
FIG 10.	SEGMENTED HEIGHT DATA [SUVEG AND VOSELMAN 2004].....	28
FIG 11.	3D PLANE-ROOF POLYGON ADJUSTED TO DSM DATA [AMERI AND FRITSCH, 2000] .....	28
FIG 12.	COHERENT (LEFT) AND INCOHERENT (RIGHT) FACETS [TAILANDER, 2005].....	30
FIG 13.	WROCLAW, LOCATION OF URBAN AND SUBURBAN TEST AREA .....	32
FIG 14.	WORK FLOW .....	34
FIG 15.	WINDOWS LAYOUT OF DPLX.....	35
FIG 16.	MATCHING ALGORITHM OF DPCOR .....	37
FIG 17.	INFLUENCE OF INITIAL PARAMETERS FOR DPCOR .....	39
FIG 18.	IMAGE MATCHING WITH DIFFERENT HEIGHT TO BASE RELATION .....	42
FIG 19.	3D SURFACE (TOP) AND SHADOW RELIEF MAP (BOTTOM) OF MOP AREA IN SURFER.....	46
FIG 20.	ATOP PROCESSING.....	48
FIG 21.	PRIMITIVE TYPES IN ATOP .....	49
FIG 22.	OVERLAY OF MATCHED POINTS IN IMAGE 3717.....	52
FIG 23.	RMSZ FOR DSM VARIATIONS OF ABN AREA .....	54
FIG 24.	FREQUENCY DISTRIBUTION OF DISCREPANCIES DZ .....	55
FIG 25.	RMSZ FOR DSM VARIATIONS OF MOP AREA .....	56
FIG 26.	FREQUENCY DISTRIBUTION OF DISCREPANCIES DZ AS F(DZ).....	57
FIG 27.	ERRORS IN RECONSTRUCTION.....	60
FIG 28.	DEMANAL SITUATION PLOTS FOR PSEUDO DSMS – ABN AREA .....	61
FIG 29.	DEMANAL SITUATION PLOTS FOR PSEUDO DSMS – MOP AREA.....	62

## List of tables

TABLE 1 NUMERICAL CHARACTERISTIC OF THE STUDY AREAS .....	32
TABLE 2 THE CHARACTERISTIC OF THE USED IMAGES .....	33
TABLE 3 HEIGHT TO BASE RELATION FOR TESTED AREA.....	40
TABLE 4 NUMBER OF MEASURED POINTS.....	44
TABLE 5. OVERALL CORRECTLY MATCHED POINTS .....	51
TABLE 6. DSM ACCURACY RESULTS FOR TEST AREA ABN.....	54
TABLE 7. DSM ACCURACY RESULTS FOR TEST AREA MOP .....	56
TABLE 8. ACCURACY OF THE GENERATED BUILDINGS MODELS .....	58

# **1. INTRODUCTION**

## **1.1. Objective of work**

This thesis has task of proving that a multipurpose data source, which digital images are, can provided in an automatic way not only accurate altitude model, i.e. digital surface model, for dense urban area but also three dimensional buildings, since there are the most desirable part of city models. The research focuses the attention on the 3D building reconstruction form cadastral data base and aerial images and inherits for the method proposed for data obtained from airborne laser scanner. The assessment the usefulness of UltraCam<sub>D</sub> images for the stated task takes under consideration in the first place feasibility and efficiency of the approach, and then the geometrical accuracy of the results is estimated.

## **1.2. Scope of work**

Experimental analysis was carried out using digital images, which were acquired for municipal authorities of Wroclaw from UltraCam<sub>D</sub> camera. The image acquisition took place in May 2006. Since the local geographic information system was brought up to date, thanks to the obtained aerial images, the building data base was used to supply ground outlines for the reconstruction process. The panchromatic bands of two stereo pairs were processed during the research. Three dimensional solid buildings were reconstructed on basis of two data types extracted form digital images, i.e. the evaluated digital surface model and the buildings outlines.

The data sets utilized in the thesis were available thanks to the Tele Atlas Sp. z o.o. company and are samples of a regular-carried out production tasks.

## **1.3. Motivation**

The growing demand for the up-to-date and reliable, also spatial, information so typical of the era of global communication, made real explosion in a market of Geographic Information Systems (GIS), which are already casual for information society. It is maybe to early to announce the end of the printed-map era (e.g. in the city planning large format of a map is continually essential) compared to digital presentation, but indisputable remains the fact that the utilization of 3D GIS is becoming more and more important for representation of and analysis of spatial information, particularly essential on municipal terrains [Danahy, 1999].

For years presence of the technology GIS, its creators convinced that every user would understand the two dimensional display of information. However, the world around us is three-dimensional and it seems natural that the presentation of data from GIS should go toward that direction.

Though manual techniques of 3D data acquisition are well-known, with regard to their time consuming and expensive process, are ineffective in build up areas. Therefore, several research projects aims to automate this process.

Most of the building reconstruction strategies have two main parts: the localization step and the reconstruction step. The localization of the building in the images means the detection of regions of interest where the buildings lie. By first localizing the buildings in the images, the reconstruction process can be focused on one building structure. This reduces the complexity of the reconstruction by a large amount. Thus, it is desirable to localize the buildings in the images first and to do the actual reconstruction afterwards. While the detection problem is rather two dimensional, the geometric reconstruction is a much more complex task for automatic algorithms. These complexities led to the increased use of building layers often available cadastral systems, which support 3D reconstruction essentially. The strategy proposed in the theses becomes part of this context.

## 2. THEORETICAL SECTION

### 2.1. Three dimensional city models

It is not so easy to find a proper definition of 3D city model, which satisfies all, the requirement for data acquisition and the users. Although it can be stated that the three-dimensional city model is a digital description of the terrain, buildings, vegetation and streets objects in urban areas. Survey shows [Fuchs et al., 1998] that for 95% of responders the most valuable information from 3D city models seems to be buildings. Thus, almost all researchers, e.g. Jibrini et al. [2000], Ameri and Fritsch [2000], Haala and Brenner [1997], focus on automation of building extraction. However, it is worth to stress now that aerial images are able to provide all components of a city model in one data set.

#### 2.1.1. Data sources

As many solutions of automatic of three-dimensional data generation, so many are initial data sources. The automatic data acquisition from different sources is in a high level of implementation. However, the most difficult part of the automation process is the acquisition of reliable geometric data in dense urban areas. There are three general of data sources used for automatic reconstruction of three-dimensional buildings. Brenner, [2000], suggests the following division:

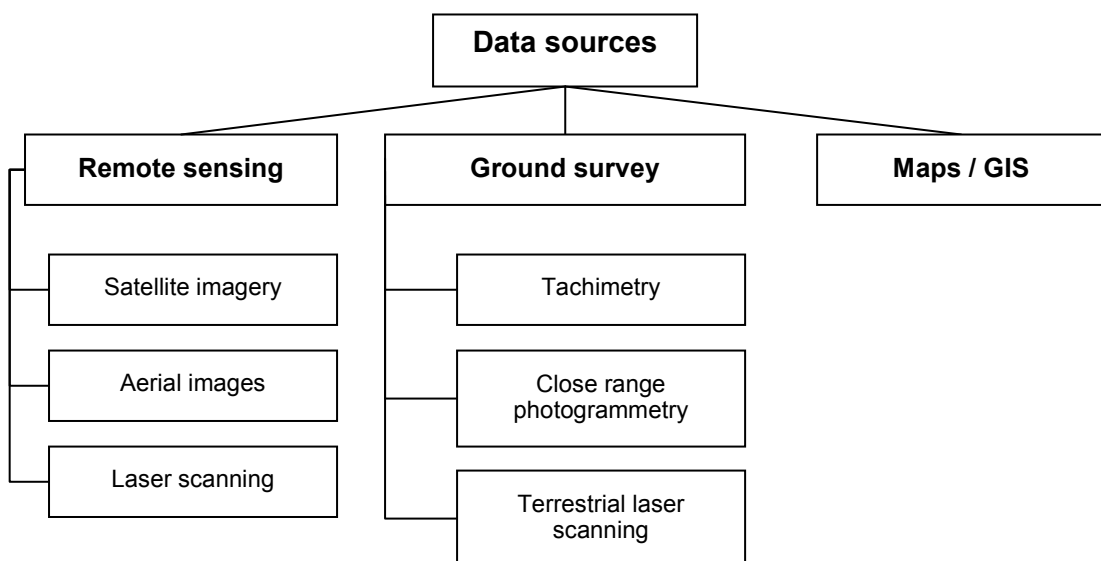


Fig 1. Data sources

## **Close range**

The measurements carried out with terrestrial techniques may lead to more detailed models. In fact, they are the main source of photorealistic textures and the precise data about buildings' walls besides oblique aerial images. Usually the combination of a laser scanner and sets of high-resolution camera is used for the automatic extraction of 3D models from terrestrial measurements. If they are mounted on mobile vehicle (a car, a railway engine), these instrument's combinations are named Mobile Mapping Systems (MMS). A good example of this kind of approach is presented by Früh and Zakhor [2001]. However, 3D model obtained by data from the MMS data can be incomplete, due to lack of roof shapes and sometimes gaps in building's height data, which are more relevant part of 3D models for many applications. Thus, measurements from the ground level, even if highly automated, may be only a supplement for data acquired from aerial and space platforms. Moreover, the terrestrial technologies are still less efficient, even with consideration to mobile platforms. Also the level of automation is still unsatisfying. Caused by high expenses, this data source is rather rarely taking into account for automatic production of 3D city models.

## **Aerial laser scanning (ALS)**

Several current research projects on applying remotely obtained (range 500m and higher) data for 3D man-made object reconstruction, are focused on aerial laser scanning [Schwalbe et al., 2005], [Rottensteiner et al., 2005], [Vosselman and Dijkman, 2001].

The main reason for this is the fact that ALS provides dense clouds of directly measured 3D points and because of that describes well planar surfaces and sharp height changes. Thank to that, the automatic building extraction process can be more straightforward. Additionally, there is possibility to register several echoes, normally first and last, of laser pulse, which is very useful during laser data segmentation and filtering. But on the other hand points during aerial laser scanning are sampled in fixed, regular pattern, which often causes the information lost about particularly essential points, like corners, and opposite provides lots of irrelevant points noising the plane's description, like chimneys and roof furnishing. Other disadvantages of this data source is still relatively high acquisitions costs as well as low number of devices compared to aerial cameras, especially in developing countries.

## **Aerial images**

Photogrammetric technologies for processing optical imagery (aerial or space images) are well known and still they are developing towards full automatic acquisition of data, especially three dimensional. The breakthrough in automation process came in the early 90's

of the last century, when the automatic image matching became commonly used. Simplification of 3D primitives' extraction and the new algorithms in digital image processing led to research of automatic man-made object extraction from very high-resolution images [Gruen, 1997], [Ameri. and Fritsch, 2000], [Baillard and Zisserman, 2000]. Another giant step in data acquisition process was the invention of first digital aerial cameras like ADS 40, DMC or Ultra Cam. Thanks to very good radiometric quality (12 bits) and better contrast compared to analog images, more efficient and high quality matching can be applied by means of digital images [Leberl et al, 2003]. Moreover, without any additional costs the along-track overlap can be extended, which reduces the occlusion problem in dense urban areas and provides multi-ray matching, refining vertical accuracy [Thurgood, 2004]. Digital surface model derived from aerial images has almost similar quality as data acquired directly from ALS. In addition aerial images, unlike ALS technology, are source for not only geometrical information, but also allow obtaining descriptive attributes of objects. This multipurpose data source and can also be applied for other purpose than three-dimensional building reconstruction [Gruen, 2001].

## **Maps and Geographic Information Systems**

2D Maps and geographic data bases are quite important data source for three-dimensional building reconstruction at different level of details (LoD). GIS provide semantic information about buildings, like number of floors, which after rough estimation of average floor height can easily lead to block models. Furthermore, as it was mentioned before, the problem of automatic reconstruction is divided to two essential parts: detection and geometric reconstruction. Building ground plans lead to a huge step toward quality and efficiency of automatic process. In comparison with results of automatic detection, the outlines from GIS are more reliable, since they are collected and interpreted by human.

The external knowledge about buildings outlines simplifies several issues of building reconstruction:

- Assuming the ground plans are correct, locating the ALS data points is trivial. When using aerial images the extraction of buildings is depending upon the GSD. The uncertainty arising from the unknown building height result into small search area in the images [Suveg and Vosselman, 2004].
- The orientation of the ground plan lines can be used to constrain the normal direction of roof faces [Brenner and Haala, 1998], [Tailander, 2005], usually the normal direction will be perpendicular to one of the outline segments.

- Finally, a ground plan often reveals information on the structure of buildings. When modelling buildings by constructive solid geometry, buildings can be regarded as combinations of a few components with simple roof shapes (flat, gable, hip, desk etc.). The shape of building ground plan can be used to derive hypothesis on the portioning of a building into these building primitive [Brenner and Haala, 1998], [Brenner, 2000]

But also drawbacks of using this data source have to be stressed: some roof elements, like dormer are not represented in 2D maps and on the contrary some of the small outline elements are irrelevant to roof structures. Also in many countries the existing maps are outdated and an up-to-dated GIS does not exist. Additionally this data source is not as accurate as many approaches assume. In every procedure, where this external source is used, mentioned disadvantages must be taken under consideration.

### **2.1.2. Applications**

Experiences show that 3D visualizations have much stronger influence on decision making process, than written text, two-dimensional drawings or other tables with numerical data. In particular it refers to spatial information and this is the basis of several applications, where 3D city models are used or they can be used. During last years interest in three-dimensional models of cities increased extremely. More and more fields of life as well as a science benefit from the digitally created models. Their applications are manifold.

#### **Urban planning**

Urban planning is certainly one of the most essential fields, where three dimensional models are used. The local administration often has to face complex decision processes regarding either the reconstruction of city or large investment projects, such as new shopping centres, industrial areas etc. Thanks to possibility to handle different formats by visualization systems, architects participating in the planning process can easily present and situate the draft versions of their projects in virtual reality. Also the influence on urban scenery of future investment, as highways, it becomes more readable and clear in three-dimensional context.

#### **Engineering**

Traffic noise, is a frequent problem of large urban agglomerations. In order to assure the admissible noise level digital simulation of noise propagation can be created. It requires up-to-date spatial data base including the three-dimensional city model. In similar manner the

propagation of air pollution can be derived. This application of 3D agglomeration models was the fastest adopted by telecommunication companies, for planning of transition stations

## Tourism

Also tourists, who are planning their holidays profit of visualization tools for three-dimensional city models, based on web technologies. Since the spatial and semantic information is easily accessible, the tourists already before departure can get good impressions about their ski resort scene or visit 3D city via internet. The hotels, the restaurants with view of the sea or sightseeing trips can be simply found and booked.

On the other side of tourist 3D portals are the hotels and the restaurants owners and other vendors, who are really concern about the best recognition of their brand. The online 3D city services allow the managers to present tourist facilities including their spatial advantages. The virtual tourism is the fastest developing application of three-dimensional city models.

## Other applications

The further fields of an application for 3D city models are the real estate security, navigation, architecture, civil engineering, but also the entertainment industry, i.e. the television, cinema and computer games.

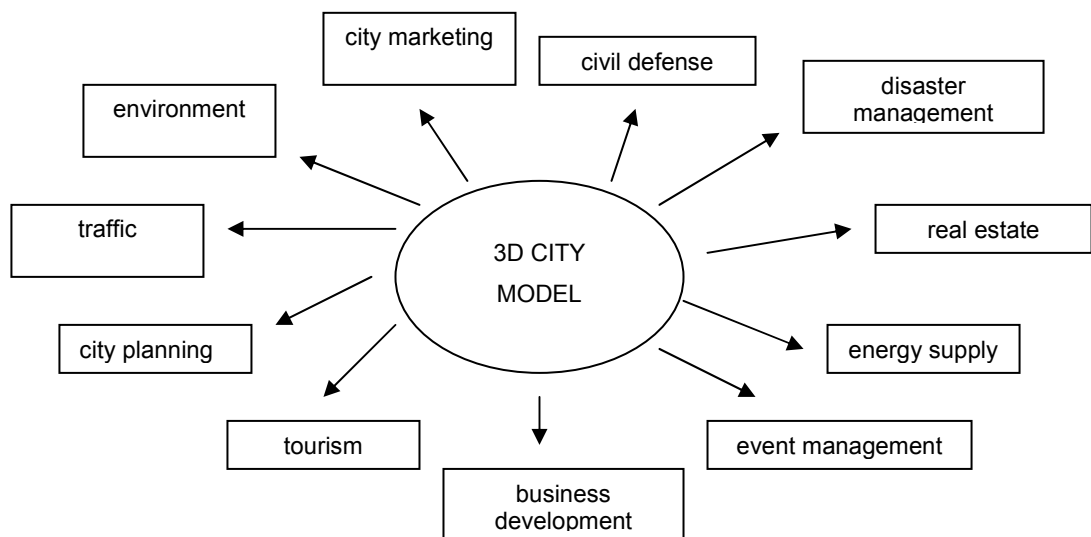


**Fig 2. Potential applications of 3D city models [Schulze-Horsel, 2007]**

Acquisition and continuous updating 3D data is much more demanding in relation to two dimensions, economic important is a high degree of automation The automation

techniques of acquisition and actualization were and are continuously object of investigations. However, as always with new technology the expectations are strongly exaggerated. It can be safely stated, that the time of automatic generation of high accurate city models fulfilling all users' requirements did not come yet

### **2.1.3. Generalization, Level of Details (LoD)**

As mentioned in previous chapter not for every application of 3D city models, the same level of information is required. Demanding three-dimensional building information with high quality of visualization are opposed to the low-quality 3D GIS data, sufficient for telecommunication or environmental simulations [Brenner 1999]. Therefore different applications of 3D GIS require different level of generalization that means levels of details (LoD).

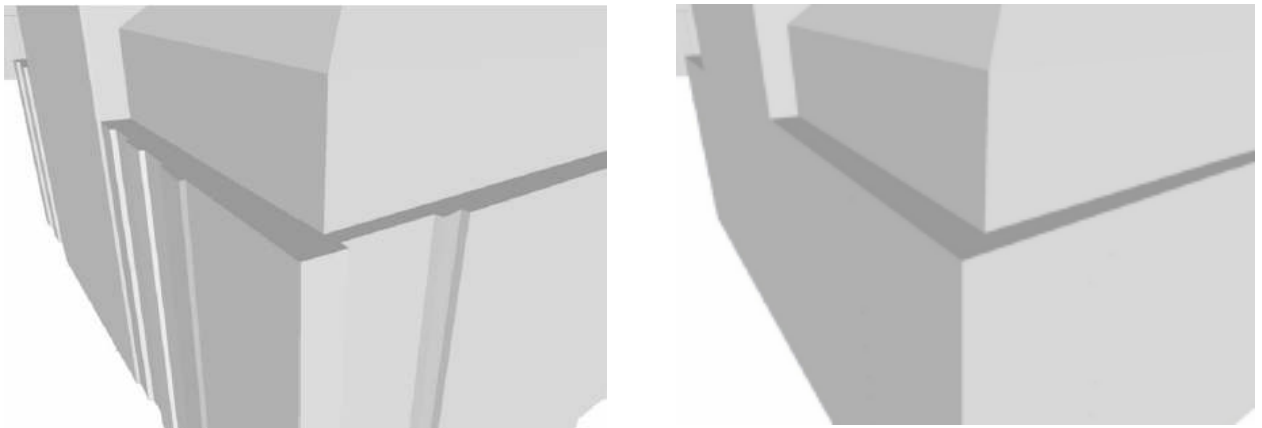


**Fig 3. Sample generalization of the building's edges [Kada, 2003]**

The Level of Details defines different visualization methods of the same object, which are different in the terms of complexity, e.g. a polygon without textures, the texturing degrees, models of lighting etc. The criteria of generalization depends on the application and it can depend on the observer's distance to the generalization object, the size of object or the eccentricity of object in relation to the user's field of view [Reddy, 1998].

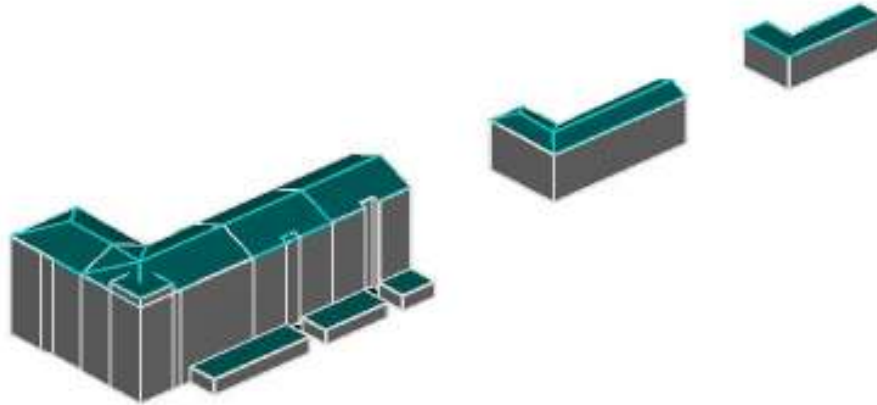


**Fig 4. Stages of generalizations depending upon distance of the observer**

In contrast to cartographic two-dimensional display, e.g. the topographic maps, where the scale's sequences as well as the generalization are well defined, the 3D city models have no unified norms of visualization. Therefore it is very hard to define the level of details of the 3D models to be produced, often even customers are not able to express their requirements. Long lasting investigations into city models resulted into a systematic of the LoD [Gröger et al., 2004], [Kolbe, 2004], [Schilcher et. al., 1998], [Thiemann, 2004], which can be helpful to meet client's needs. And though the differences among them are not cardinal, it is worth to have glance at them, since they are equally defined.

Gröger et al. [2004] describe five level of detail of 3D landscape:

- LoD 0 = digital surface model draped with map or ortho-image with land cover
- LoD 1 = building outlines extruded to unified height,
- LoD 2 = LoD1 refined by texture, roof types and vegetation feature,
- LoD 3 = architectural models with vegetation and street furniture,
- LoD 4 = architectural models with indoor features.

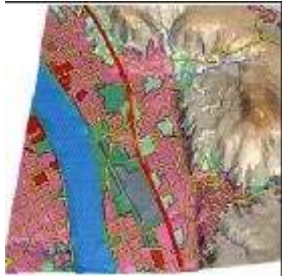
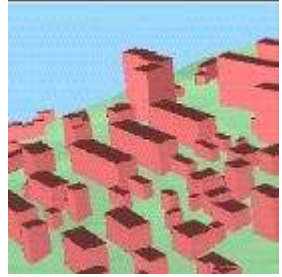
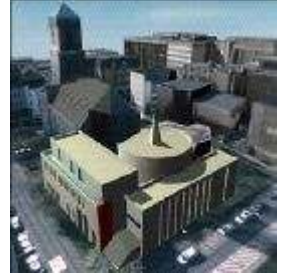
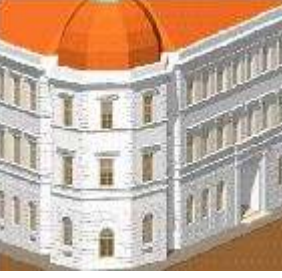
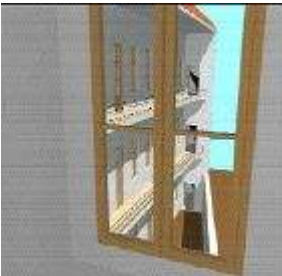
Kolbe [2004] similar to Schilcher et al.[1998] proposes following division:

- LoD1 = building outlines extruded to unified height,
- LoD2 = LoD1 improved by standard-roof shapes with simulated wall texture,
- LoD3 = LoD2 improved by detailed roof structures and photorealistic texture.

While Thiemann [2004] introduces level of urban area as follows:

- LoD1 = aggregated buildings with uniform height ,
- LoD2 = solid separate structures with flat roofs,
- LoD3 = LoD2 refined by simplified roof structures.

While languages as well as systems describing virtual reality, e.g., VRML, Autodesk 3DS, X3D, present the wide range of general graphic functions, then however they do not provide the proper means to describe 3D geodata. Therefore it is required to use semantic description of 3D objects. The idea to unify the definition, description and method of modelling the three-dimensional cities' reality led to the CityGML initiative [Kolbe et al., 2005]. It resulted in concept of unified notional model and description format (GML language) of geodata regarding 3D urban environment. Since the model can be used to spatial analyses and queries, the whole potential of generated 3D product finally can be applied, while it is often relegated to just visualization purpose. Among many other specifications of 3D models, the levels of generalization are also defined by the project coordinators. Implementation and using the unified system of level of details will allow the sufficient comparison of three-dimensional city models as well as the integration of different 3D data sets. Since the CityGML language is adapted to the below performed division of the LoD, it is widely applied in the production, what confirm success of the CityGML initiative.

LoD 0		<p>Digital surface model draped with a map or an ortho-image. Accuracy of XYZ coordinates higher than 5 m.</p>
LoD 1		<p>Building outlines extruded to unified height. Accuracy of XYZ coordinates better than 5m. Features with outline smaller than 6x6 m are not reconstructed.</p>
LoD 2		<p>Various roof types with textures, vegetation (trees) can be also be presented. Accuracy of XY is 2 m, of altitude 1 m. Features with outline smaller than 6x6 m are not reconstructed.</p>
LoD 3		<p>Architectural models with detailed walls and roofs shapes, including photorealistic textures, with vegetation and street furniture. Accuracy of XYZ coordinates is 0.5 m, minimal outline of displayed objects is 2x2 m.</p>
LoD 4		<p>Fills the LoD 3 with indoor features, e.g. floors, rooms etc. Accuracy of XYZ coordinates is 0.2 m and better.</p>

**Fig 5. Level of Details according to CityGML**

## 2.2. Automatic image matching

In order to obtain any three dimensional information for images, e.g. digital surface model, conjugate points must be found in overlapping images taken from different directions.

The term of image matching is connected not only and exclusively with digital images and photogrammetry. In general, the matching of images is based on finding the corresponding points in images, which represent the same object. This process is incessantly set in human brain, in view centre, which unites images registered by right and left eye, enabling the three-dimensional perception of space for human. This natural fit of images is used in classic analogy photogrammetry during the stereoscopic observation of stereo models.

The matching technology with reference to a pair or more images is used for 3D surfaces reconstruction on a basis of two dimensional images. Parts of information are lost during image acquisition process. This fact is due occlusions in both images, multidetection caused by repeatable structures, unstable solution as result of radiometric or geometric noise. Refinement of matching process is performed by adding some extra information, such as:

- changes in object illumination and influence of other atmospheric effects may be reduced thanks to near simultaneous acquisition,
- assumption that imaged objects are characterized by their geometrical relations,
- objects surfaces are fragmentary planar, opaque and some of their characteristics e.g. diffusion of lighting are repeatable in both photos,
- start rules, required especially in a rough area, are known.

Following described methods, especially the last mentioned point, specifies the efficiency of an algorithm. The chose method may be rather essential.

The classification of matching methods is conducted by analysis of:

- a form of primitives selected for feature extraction,
- kinds of models (geometric or radiometric) used to match primitives in the images,
- ways of finding similarity between recognized features in overlapping images and determining the optimal similarity,
- which strategy is performed in order to control matching algorithm.

The aim of the automatic image matching is the identification of corresponding points (elements or details) in the both images. The matching can be grouped into Area Based Matching (ABM) based on the grey values of the sub-matrixes and Feature Based Matching

(FBM) using local features (a point, an edge, a line segment or small regions) but also global, elements like polygon, complex shape.

### 2.2.1. Area Based Matching (ABM)

In area-based methods, the measure of the similarity is a quantity of difference between values of corresponding monochromatic pixels. In case of multi-spectral image one band is used for matching purpose. The matching primitive in case of ABM is small matrix composed of pixels' grey values. The small image parts (patches) are compared, and then their similarity is measured based on correlation coefficient or the least-squares adjustment. Image matching using correlation score is simply called Image correlation, whereas the other one is noted as The Least-Squares Matching (LSM).

Since area-based matching demands very good approximation, localization of a search matrix is rather essential. Its size is not so important, because necessity of approximation reduce the problem to size of few pixels.

Regarding to the large size of aerial image, the task of searching for the equivalent window in the second image can be very time consuming. Therefore, in order to reduce computation time, four common strategies are used. These methods use parameters of the exterior orientation to restrict the location of the corresponding position.

- **The epipolar-line method** is based on the epipolar plane, which is defined by the projection centres and the object point. The epipolar lines are the intersection lines between epipolar and image plane. After the relative orientation the epipolar images are generated. The corresponding points have the same y-coordinates in the epipolar images. Thus, the search problem becomes one dimensional.
- **The hierarchical approach** of matching reduces the search area by increasing size of pixel. For this, the images pyramids have to be generated.
- Another geometrical method for identification of corresponding location is **the Vertical Line Locus (VLL)**. After the relative orientation process, a sub-matrix in object space with X and Y as centre position can be transformed to the stereo pair. Changing the value of Z coordinate, the algorithm compares the corresponding image matrixes. Since the object coordinates X and Y can be fixed prior to the matching, the predefined grid model is generated. That gives this method the advantage over epipolar-lines method.
- **The Region Growing** algorithm uses the pixel positions of manual measured control and tie points as start values. The corresponding points are determined by a combination of image correlation and least squares matching. The image

matching is handled in the image space. Starting from known corresponding points, other homologue points are identified in the neighborhood and from these again other points are identified up to the covering of the whole model. This method has the advantage that it is not necessary to modify the matching program for the special image geometry.

### Image correlation

In this method, based on relative differences of intensity between corresponding sub-matrixes in both images, the location in the search matrix is estimated, which gives the highest similarity to the reference sub-matrix. The maximal correlation coefficient specifies the best fit of the sub-matrixes. The correlation coefficient is a measure of relation between two random variables. It is defined as a ratio of the covariance to the square root of the variances product:

$$\rho = \frac{\text{cov}(X,Y)}{[\text{var}(X) \text{var}(Y)]^{1/2}} \quad (1)$$

The correlation would be perfect (equals 1), when the two sub-matrixes would have the same grey values. Beside radiometric differences this is only possible for horizontal plane object area. In case of no correlation the coefficient equals 0, while -1 value means reverse correlation, when the negative and positive images are compared.

Due to object undulation the compared sub-matrixes have to be reduced in size, to provide feasibility of the matching process. Additionally, in order to free the correlation coefficient from the local changes of brightness and contrast in the image patch, the equation (1) is normalized. Therefore the normalized cross-correlation coefficient in detail is express as:

$$\rho = \frac{\sum_{i=1}^M \sum_{j=1}^N (g_1(i, j) - \bar{g}_1)(g_2(i, j) - \bar{g}_2)}{\sqrt{(\sum_{i=1}^M \sum_{j=1}^N (g_1(i, j) - \bar{g}_1)^2)(\sum_{i=1}^M \sum_{j=1}^N (g_2(i, j) - \bar{g}_2)^2)}} \quad (2)$$

Where:

- $i, j$  – number of row and column in the template matrix,
- $M, N$  – number of rows and columns in the template matrix,
- $g_1(i, j)$  – grey values in the template matrix,
- $g_2(i, j)$  – grey values in the search matrix,
- $\bar{g}_1$  – mean of grey values in template matrix,
- $\bar{g}_2$  – mean of grey values in the search matrix.

In order to compute cross correlation, in one image the window template area  $N \times N$  and in second search area  $M \times M$  are chosen, where  $M > N$ . The correlation is computed between window area and search area, in the centre of search area  $L \times L$ , where  $L = M - N + 1$ . Computation of the correlations for every  $L^2$  shift possibility needs for  $L^2 \times N^2$  operations. As Jacobsen [2006] mentions the size of search matrix should not be too small to avoid problems caused by not accurate initial values and it should not be too extended to avoid a second maximum.

The position, where the correlation coefficient gives maximum value is chosen as the best match between the template and the search area.

Only pixel accuracy can be achieved using the cross-correlation matching, thus it is usually applied for a rough localization of matched points to performed LSM afterwards

### **Least-Squares Matching (LSM)**

The image matching with normalized cross-correlation coefficient of the grey values of the same object in two images is based on the hypothesis of horizontal location of the matched areas. So by theory cross-correlation is correct only for horizontal objects, because sloped elements have different size in the corresponding images. Therefore another area based approach was proposed with the Least Squares Matching [Ackerman, 1984].

In this approach the principal rule is to compensate the normalized radiometric and geometric differences of two sub-matrixes by minimizing the differences in grey values by transformation of one sub-matrix to the other.

The grey values in the matched windows are approximated by function of pixel coordinates and assumed to be located on a tilted plane surface. The relation between these two functions, i.e. grey values in left and right image, can be described as affine transformation considering also linear radiometric distortion. The geometric transformation can be noted like following:

$$X'' = a_0 + a_1 x' + a_2 y'$$

$$Y'' = b_0 + b_1 x' + b_2 y' \quad (1)$$

where:

$a_0 \dots a_2, b_0 \dots b_2$  – geometric transformation parameters

$X'', Y''$  – the coordinates of matching sub-matrix

$x', y'$  – the coordinates of search sub-matrix

In addition to the geometric transformation also a compensation of linear variations of grey values is respected. The radiometric transformation between template and search window is expressed by following formula:

$$g'(x', y') = r_0 + r_1 g''(X'', Y'') \quad (3)$$

where:

$r_0, r_1$  – radiometric transformation parameters

$g'(x', y')$  – grey value in the matching matrix

$g''(X'', Y'')$  – grey value in the search matrix

Finally the relation of the grey values of corresponding sub-matrixes is as follows:

$$v(i, j) = r_0 + r_1 g''(a_0 + a_1 x' + a_2 y', b_0 + b_1 x' + b_2 y') - g'(x', y') \quad (4)$$

By minimizing the square sum of residuals  $\sum v(i,j)^2$ , the unknown parameters for geometric and radiometric transformation can be adjusted, thus all pixels in the search window become conjugate with the template window.

The least-squares image matching is the most accurate method, but it has the disadvantage of a small convergence radius – the approximate relation between both images must be known in advance. Thus it has to be combined with a method giving approximate conjugate positions [Jacobsen, 2006].

### 2.2.2. Feature Based Matching (FBM)

In this matching group, the following entities can be used for local investigations: points, edge elements, line segments, small areas, and for global - polygons and more complex structures, which are usually sets of elements mentioned before. The entities should be independent from radiometrical distortions and image noise and they should be rare in used images.

Every feature is described by the set of attributes. The main attribute is a position of a feature in image co-ordinates system. Additional attributes can be - the direction of a line, the distinctiveness of an edge (the brightness gradient of pixels calculated crosswise to edge), the length and the curvature of a line or a group of segments, size and an average brightness of a polygon.

Global features are usually groups of different local features. In this case attributes defining geometric or radiometric relations between local features are taken under consideration. Therefore global feature matching is often called relation matching.

The result of feature extraction is the list of features and their attributes defined for each image. In next processing step, only such lists are analyzed. The Feature is a discrete function of geometrical position (after feature recognition it is essential whether it occurred in this position, whether not).

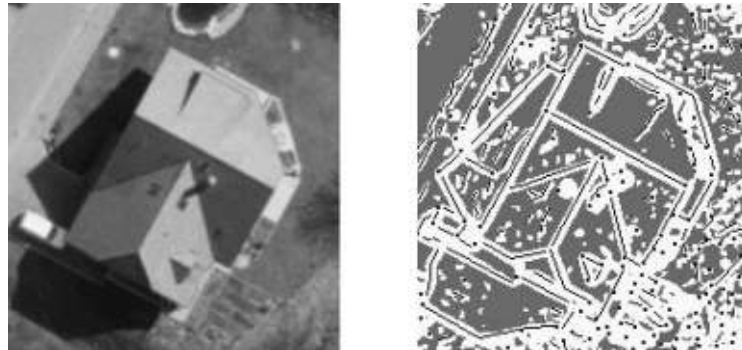


**Fig 6. Aerial image and corresponding image features [Foerstner, 1999]**

Local-feature-based methods were quite success in many image processing issues including scene reconstruction, object extraction and registration. The main idea is to concentrate efforts on a relatively sparse set of particularly essential image elements, also called interest points, which are specified by interest operators. Different interest point extractors have been proposed. Some detectors search for points of high local symmetry, others find areas of highly varying texture, while others locate corner points. Corner points are interesting as they are formed from two or more edges and edges usually define the boundary between two different objects or parts of the same object. Many interest operators have been developed like the popular Moravec operator and Foerstner operator.

### **Moravec Interest Operator**

The Moravec Operator is a corner detector as it defines interest points where large intensity differences in every direction occur. In small square windows directional variation is estimated. Square sums of differences of pixels adjacent in each of four directions (horizontal, vertical and two diagonals) over each window are calculated, and the window's interest measure is the minimum of these four sums. Features are chosen where the interest measure has local maxima. The feature is conceptually the point at the centre of the window with this local maximal value.

### **Foerstner Interest Operator**

The Foerstner interest operator is used as first step for Forstner's feature-based image matching algorithm. The Foerstner operator selects points such that they fulfil

requirements like distinctiveness, invariance, stability and interpretability. This interest operator at first selects optimal windows based on the covariance matrix and then selects an optimal point within each window and then a measure for seldomness is applied to the selected points to satisfy the requirements for point selection. Since the operator is coupled with the image matching technique, it uses the two scenes together to select the points and uses the information derived in this process for matching the two images. This algorithm is very popular among the computer vision groups.

In comparison to area based matching, the FBM methods are more invariable in respect to location or radiometrical distortions. Moreover, the matching based on features is more adaptable to cities with sharp edges and do not require good approximations. However, FBM efficiency is strongly related with end product of the feature extraction process. And since in the aerial photos only a restricted number of well defined features are available, this is not enough for generation of a digital surface model. Thus, the matching based on features is commonly used as an initial value for other methods requiring some approximations.

## 2.3. Automatic extraction

In the literature there are two general approaches of the building reconstruction from aerial images: model based and data based.

### 2.3.1. Model based methods

The first one is based on external knowledge about building shapes (model based), it tries to adjust parametric building models from a limited domain of known building types (gable, hipped, cone, flat etc). This approach is intrinsic connected to the way of 3D reality modelling called Constructive Solid Geometry (CSG). CSG allows the creation of complex surface or objects by making Boolean operators on simple solids. The three main Boolean operators are:

- Union ( $\cup$ ) – the resulting solid corresponds to the all volume from the operand solids
- Intersection ( $\cap$ ) – the resulting solid corresponds to the coincident volume the operand solids
- Difference ( $-$ ) – the resulting solid corresponds to the volume from one of the operand solids outside the other ones.

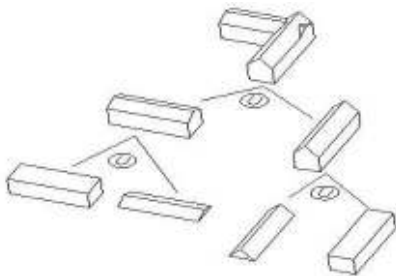


Fig 7. CSG reconstruction tree

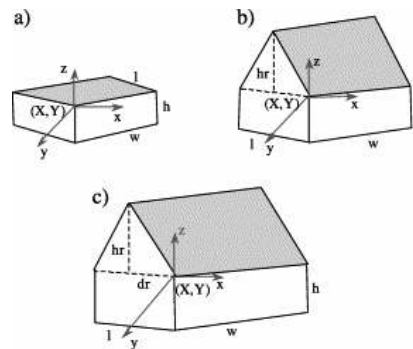


Fig 8. Parametric description of the primitives

[Suveg and Vosselman, 2004]

A solid in CSG notation is represented in function of the primitives and operations used in its composition. Solid modelling performs well in automatic building reconstruction, in particular it corresponds properly with simple-shaped objects showing symmetry, which can be described as combinations of a few basic components, primitives. The primitive can represent a building or a part of building depending on the complexity of building shape. For instance a cuboid building can be represented by solid box with parameters of length, width

and height. In order to adjust the prior-declared primitives, the outlines segmentation into rectangles needs to be performed. Since the generated rectangles are considered as footprints of models, subdivision of ground plans has crucial influence on the results.

### **Brenner and Haala, 1998**

The authors used a DSM in a raster format and building outlines from GIS as external data source. Although, originally they applied the height values from laser scanner, and aerial images for a posterior semiautomatic edition of objects, it has to be said that nowadays similar DSM can be extracted by automatic matching of digital aerial images.

Two-dimensional outlines are assumed to be precise and partitioned into rectangles using a heuristic algorithm, in the first step of reconstruction. Every rectangular segment of ground plan is considered separately as an individual primitive. After segmentation of the raster height data to planar patches, comes the adjustment of the model in relation to the library of building types. The right model is chosen based on the best score of minimization process (using the least-square method) of the distance between the DSM planes and the corresponding segments of a primitive wireframe. And the final representation of complex building is a combination of primitives described as CSG tree.

### **Fischer et al., 1998**

One of the earliest approaches to the automatic building extraction was developed at Bonn University and it uses model-based description of real buildings, where primitives are buildings parts, in particular either terminals or connectors of simple buildings, both parametric models.

Firstly, the image features like points, edges and small regions are extracted. Then corners are searched for in all images, which are promising for 3D reconstruction. The generated 3D corners are indexed with respect to typical building corners. Next follows an aggregation of the corners into object parts, in this case into simple building primitives called 'connectors' and 'terminals'.

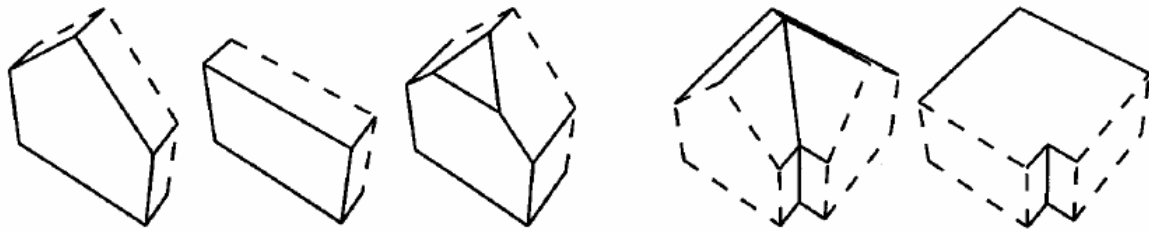


**Fig 9. Terminals (left) and connectors (right); plug faces, which are used to connect them, are drawn dashed. [Fischer et al., 1998]**

A 3D analysis of the building yields situations where a) neighbouring corners belong to the same building primitives, fixing some of their parameters of these primitives and b) neighbouring corners linking different but compatible building primitives, fixing parameters common to both primitives. In the final step the buildings models are extruded to the height taken from Digital Terrain Model.

#### **Suveg and Vosselman, 2004**

This approach uses aerial images, and as a second data source, 2D ground plans. The process is fully automated and consists of seven general steps. Despite the fact that GIS data considerably restricts the number of solutions, they are not assumed as exact by the authors of the method. First step is rough estimation of building height by back projection of an outline to the image. Moving the ground plan along epipolar line the estimated altitude is evaluated, which is based on the length of a line, extracted from the image within the back-projected building ground plan. As next the building footprints are divided into rectangular segments, handled separately from now on. In the third step, the 3D corners are generated, using feature based image matching. Moving to the fourth part of the method, for the information about the 3D corners the size of a ground plan segment is used in order to adjust the parametric model of a building, including the primitives' library. The precise parameters of the building are estimated by adjustment with the least-squares method of the back-projected model into the gradients of image pixel along the wireframe.

Two methods are used to assess the accuracy of the reconstruction process: summed up value of gradient measured along projected contours of the model and score of pixels' intensity matching of both images. Finally, all of the buildings primitives are adjusted once again, considering the geometric relations among them, e.g. common corner or edges, which are entered as the weighted constrains to adjustment process.

The result of experiment is 70 % of proper reconstructed buildings in the tested urban area. However the authors points two general drawbacks of the approach: to many

segmentation hypotheses, because only building outlines were considered in the process, without imagery data and the difficulty with small primitives fitting, due to lack of sufficiently accurate line extractions.

### 2.3.2. Data based methods

The second more generic approach of automatic 3D object generation is based on data, appropriately acquired from images. Data based methods use one type of primitives, in mostly cases these are planes, which are fitted to the image data, e.g. planar patches and 3D corners. Height data can be proceeded during segmentation into homogeneous regions. In this case the analysis of surface curvature or distance of the subsequent pixels forms an initial plane [Brenner 2006]. Also the radiometric values are directly taken into the account [Ameri and Fritsch, 2000]. Another interesting method of data aggregation algorithm, known from 2D image processing, is the three-dimensional Hough transform to detect planes in an image [Jibrini et al., 2000], [Vosselman and Dijkman, 2001]. In stead of searching for a point on a line, the point on a plane is searched for. The Hough transform does not check whether the points that are found to be in the same plane indeed make up a continuous face. It may as well find some scattered points that are in one plane by coincidence. Hence, it often gives too many hypotheses. Regardless from segmentation process initial coplanar roof segments are merged, and hypotheses for intersection lines and/or step edges are created based on an analysis of the neighbourhood relations.

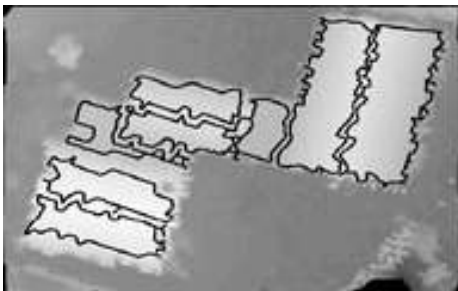


**Fig 10. Segmented height data**  
[Suveg and Vosselman, 2004]

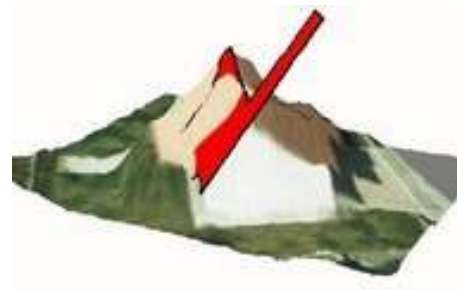


**Fig 11. 3D plane-roof polygon adjusted to DSM data** [Ameri and Fritsch, 2000]

In every data-derived method, the final product is a polyhedral building model, i.e. assuming that building is formed by planar surfaces. Thus, the models are noted in the Boundary Representation (BREP), where models are more explicit representation than CSG. The building is represented by a complicated data structure giving information about each of

the object's faces, edges and vertices and how they are combined together. Thus, not only the exact shape and position of each of the faces are stored, but also topological information about connectivity of the faces. These approaches do not restrict a building shape to prior selected models, like it is in the model based methods. By theory it has no dependency on ground plan and every man made structure can be modelled using BEREP and data based approaches.

#### **Baillard and Zisserman, 1999**

An example of data based approach is proposed by Baillard and Zisserman [1999]. It is based on obtaining half the planes from left and right side of a detected three dimensional line segment. Thanks to the delineated planar patches a polyhedral building model can be reconstructed. Typically four to six overlapping high resolution images are used.

Using Canny edge detector, as first step 2D line segments are extracted, separately for each image. Then, based on geometric and photometric information from all images the 3D line segments are produced. The facets to the left and right of each line segment are derived. In the next step the half planes, described by the three-dimensional line segment are computed. This is done by estimation of their slope, based on weighted correspondence measurements over the images with known exterior orientation. The angle with the largest score is taken. In order to reduce the overall number of planar facets, i.e. to group line segments and half planes, the collinearity and coplanarity constraints are used. Moreover, further lines are extracted by intersecting existing planar patches and the extent of each patch is obtained from a heuristic grouping. Finally each planar surface is verified by assessing intensity similarity over all images.

#### **D. Flamanc et al., 2003**

This approach, like previous model, uses GIS with building data base for refinement of a reconstruction process. It is proposed to reconstruct each building separately. At first the authors are focused on simple symmetric roofs. They determine planar surfaces by delineating an edge, which divides the 2D outline in two symmetric building halves. This assumption generates a tree of roof types, with combinations of the initial outline used for three-dimensional building reconstruction. For complex buildings, i.e. with an odd number of corners, for which the symmetric edge cannot be found, the roof faces are generated using a 3D Hough transformation, as Jibrini et al. [2000] proposed. As result an enormous number of hypothesis is obtained, which forces the use of restriction algorithm. In order to choose the correct hypothesis, the pseudo DSM is calculated from roof surfaces. By each step, a more precise DSM is computed in a volume limited by the plane hypotheses. After this, all the

hypotheses are weighted in regard to their distance to this DSM, and the worst plane hypotheses are suppressed. By analysis of the generated form planes structuring roof surface graphs, the best solution is chosen.

The authors mention the results of automatic process as follows: 50% of buildings with an easier method, 25% with data-based approach, which gives in summary 75% of automatic rebuilt objects over urban area. Additionally the evaluated height and planimetric accuracy is less than 1 m, despites that building models have low level of detail (LoD 2).

#### F. Tailander, 2005

This method uses two-dimensional information about buildings in combination with high resolution aerial photos. Opposite to other data based approaches [Flamanc, 2003], [Vosselman and Dijkman, 2001], planes are deducted exclusively from buildings outlines, without any data segmentation. At first, the planar structures are delineated from every outline segment, with two fixed parameters: slope  $\alpha=45^\circ$  and gutter height  $z=0$  m. Their intersections divide planes to oblique facets with normal vector pointed upwards. Three dimensional graphs are composed by the intersections. Using four conditions describing the roof surface model, 3D graphs can be written as assignment graph. The graph is analyzed by algorithm, which searches the admissible planes, i.e. continuous, consisted of coherent facets, which horizontal projection cover overall building outline.

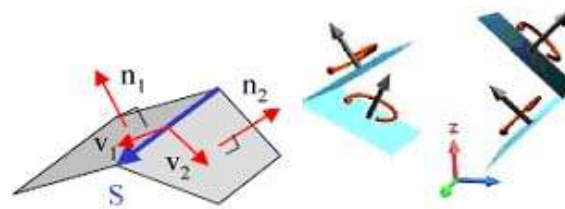


Fig 12. Coherent (left) and incoherent (right) facets [Tailander, 2005]

Following the model probability based on three conditions is computed. A model is rejected, if at the least one facet:

- is smaller than  $1 \text{ m}^2$  or two adjacent elements build an angle  $<10^\circ$ ,
- is not connected to a facade defined by outline,
- does not touch an outline segment, which the plane it lies on, has been inferred.

For every variation from the restricted number of roof surface models, pseudo DSM is generated, based on vertical distance between a roof point and a segment, from which the

plane was derived. The highest correlation coefficient, between pseudo DSM and DSM acquired from aerial images, point out for the best representation. Finally the method estimates parameters for every façade, i.e. slope and height, by minimizing the difference of pseudo DSM and reference Digital Surface Models

Based on visual inspection the following conclusions are stated. Over 90% of buildings were properly reconstructed, with toleration an assumed level of detail, i.e. lack of small details like chimneys or dormers. Vertical accuracy of the model is named with RMSE = 0.7 m.

### 3. EXPERIMENTAL SECTION

#### 3.1. Test area

The test area is located in Wroclaw (Breslau), Poland. Wroclaw is the fourth largest Polish city, with a population of 650 000 on 114 km<sup>2</sup>. The selection criteria taking under consideration was different complexity levels of its buildings. In order to distinguish between dense urban and suburban buildings, two separate city districts were chosen.

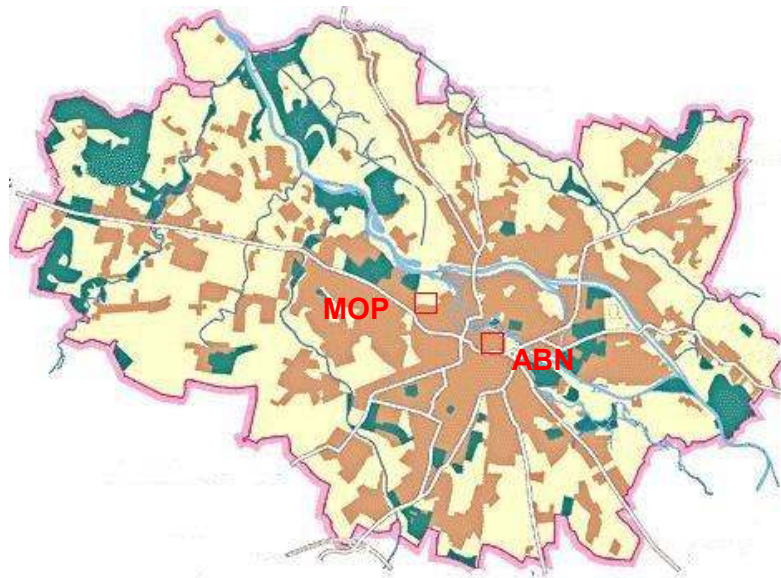


Fig 13. Wroclaw, location of urban and suburban test area

Following table shows the characteristics of the chosen districts. As it can be seen the MOP area has fewer buildings per square meter.

Area name	Area [m <sup>2</sup> ]	Number of ground plans
ABN	24 7250	147
MOP	28 6832	60

Table 1 Information about the test areas

Digital aerial images from Vexcel UltraCamD camera were used for the investigation. In addition a GIS data base containing the building ground plans, derived from the aerial images, were used. The 4724 images were captured in order to generate up-to-

date GIS for the Wroclaw local authorities. The bundle block adjustment was carried out with following results not larger than  $RMS_{XY} = 0.05$  m,  $RMS_Z = 0.07$  m. The building vector data were digitized by professional technicians with approximately 10cm planimetric accuracy.

<b>Spectral band</b>	Panchromatic (PAN)
<b>Radiometric resolution</b>	12 bits
<b>Focal length</b>	100.4 mm
<b>Image size</b>	11 500 x 7 500 pixels
<b>Pixel size</b>	9 $\mu$ m
<b>Ground Sampling Distance (GSD)</b>	0.09 m
<b>Acquisition date</b>	May 2006
<b>Overlap</b>	60 %
<b>Average flying height</b>	1000 m
<b>Coordinate system</b>	PUWG 2000 (datum WGS 84)
<b>SX=SY, SZ</b>	0.05 m, 0.07 m

**Table 2** The characteristic of the used images

For the investigation following images were used:

- 3051-3054 for ABN area
- 3717-3720 for MOP area

## 3.2. Strategy

In order to generate and analyze a Digital Surface Model for the test area of Wrocław a sequence of programs was used. Some of the programs, i.e. DPLX, DPCOR, BLPRE, BLINT, DEMANAL, RASCOR, are part of the Program System BLUH. Additionally for height data interpolation and visualization the SURFER software was used and finally for the building reconstruction the preliminary version of ATOP. The strategy and the sequence of programs are presented below:

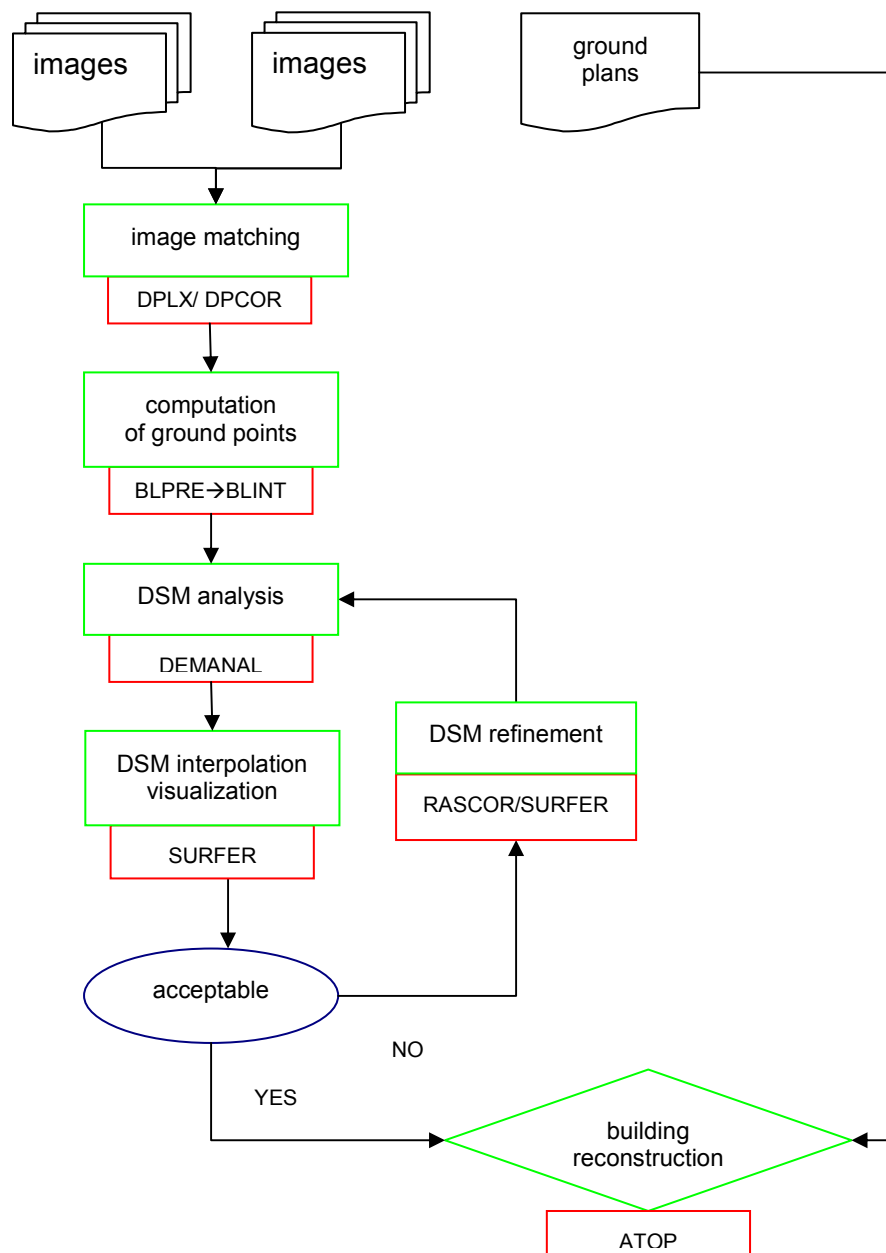


Fig 14. Work flow

### 3.2.1. Image matching – DPLX / DPCOR

The Hanover DPLX used in addition to the BLUH package, which was developed at the Institute of Photogrammetry and Geoinformation (IPI) in Hanover by Karsten Jacobsen, is intended to determine precise corresponding image coordinates in digital images. Since handling with full-resolution, large images is memory and time consuming, the original images are divided into sub-images, which can be used fast enough without problems. Raw images, \*.ima and BMP-files are accepted. DPLX was used to measure seed points, which are essential for the image matching. This step was done manually. The overview images are generated to localize the work area and zoom windows are available for more accurate point measurement. The measurements are available as image coordinates, separately for left and right image. Of course, they can be edited.

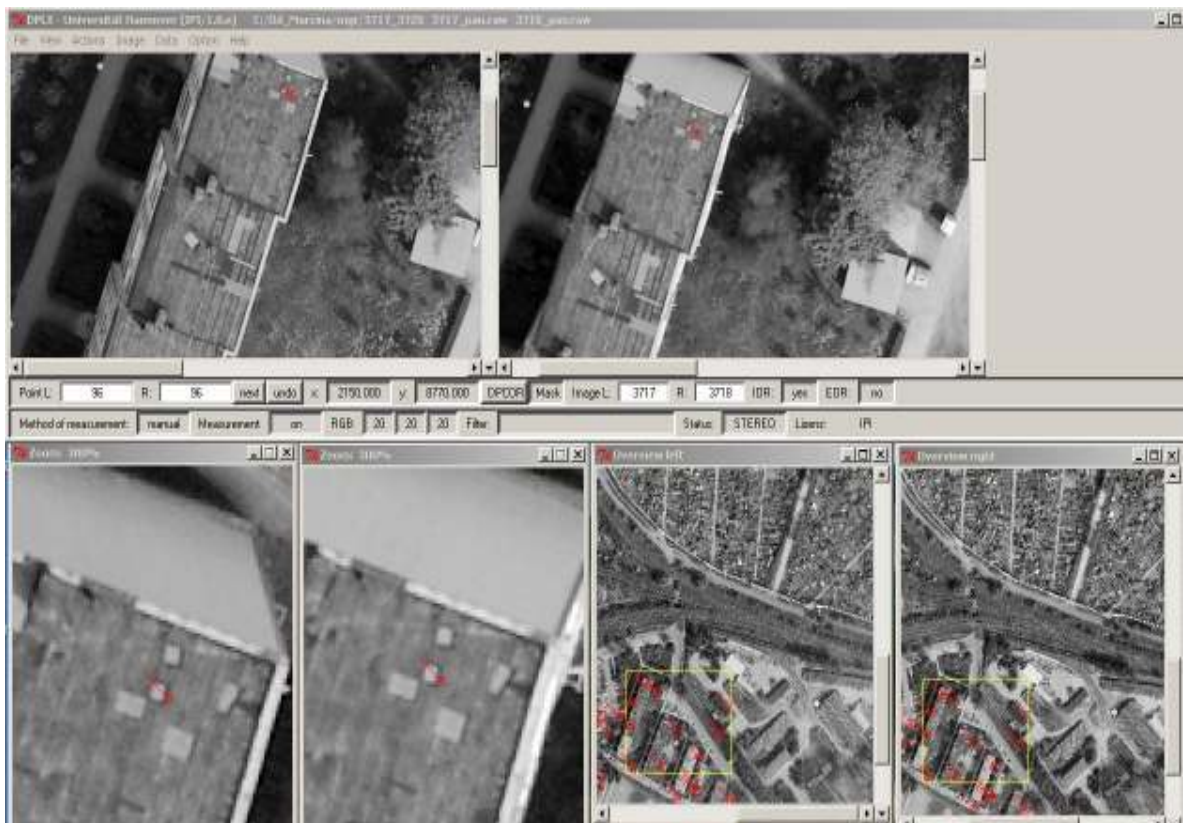


Fig 15. Windows layout of DPLX

The automatic image matching was carried out by DPCOR, embedded in DPLX. The program searches for corresponding image points within defined windows of two digital images without any information about the exterior orientation. Based on at least one seed point DPCOR is using approximate positions by region growing and determines the

conjugate positions by least-squares image matching - the by theory most accurate method. The automatic matching in the image space requires at least one start point with the corresponding positions in the both images (seed point), also control points can be used as seed points. The neighbored point of this seed point is determined by matching and it becomes seed point for the next point and thus the matching is growing over the images. The results of the image matching are pixel coordinates. The pixel coordinate system used by DPCOR has the rows from top to bottom and the columns from left to right. That means the origin is located in the upper left corner of the digital image.

The points from the left image are fixed and the DPCOR algorithm searches for corresponded points in the right image. The size of the sub matrix for matching can be chosen. The similarity of the sub matrixes is described by the correlation coefficient. For an optimal fit of the sub matrixes used for image matching, the affine transformation is used:

$$ROW_{right} = a_0 + a_1ROW_{left} + a_2COL_{left} \quad (5a)$$

$$COL_{right} = b_0 + b_1ROW_{left} + b_2COL_{left} \quad (5b)$$

ROWleft and COLleft are known, they are identical to the start position. ROWright and COLright are also at first defined by the start position, by image matching they are improved to the homologous location ROWright and COLright. For each pixel in the corresponding windows of both images the difference of the grey values are computed. A radiometric correction can be done based on an equalization of the histograms of the right image in relation to the left image. The correlation coefficients are computed using the affine transformation. If the grey values of the corresponding windows in both images are corresponding better than the pre-defined threshold, the positions are accepted as homologous. In this way the whole image will be covered using the region growing method. The matching algorithm is presented in the figure 16.

The user can define following 7 initial parameters for DPCOR:

- window size <integer>
- maximum number of iterations <integer>
- row step and column step <integer>
- threshold for correlation coefficient <double>
- radiometric normalization <Boolean>
- region growing desired <Boolean>

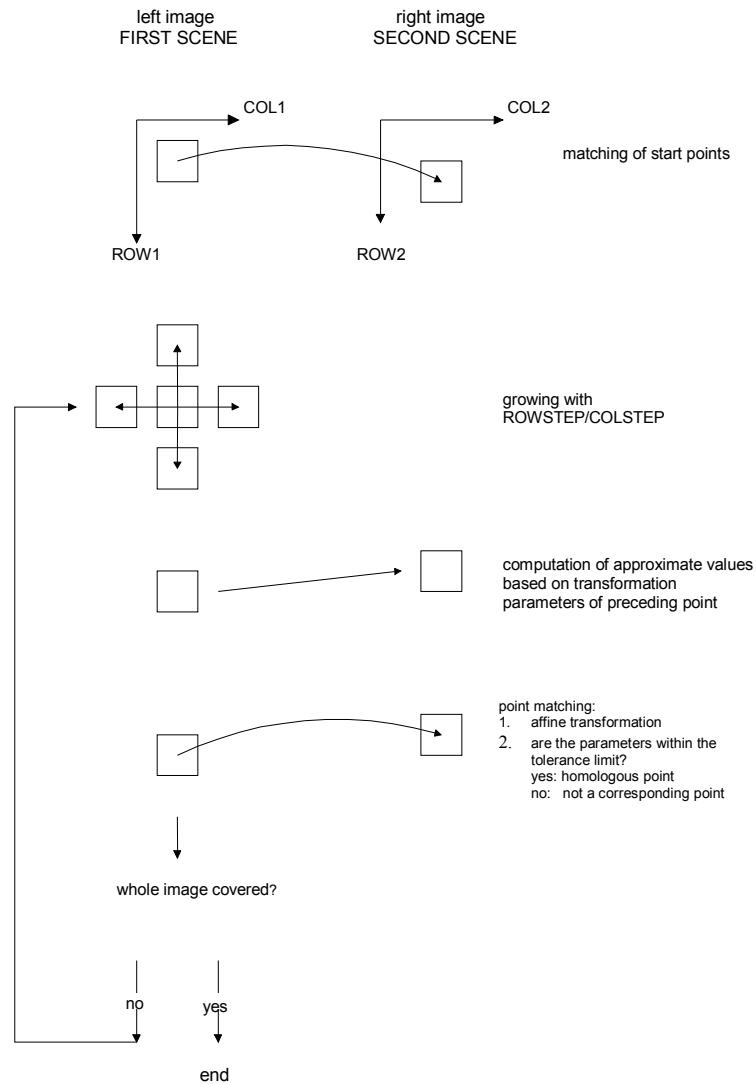


**Fig 16. matching algorithm of DPCOR**

In order to choose sufficient values of the parameters, the investigation was carried out using image samples of 1600 x 1600 pixels. If the setting *region growing desired* is set to *No* then only seed points are processed. In every case the *region growing desired* and *radiometric normalization* settings were switched on. Based on extensive experiences with DPCOR, a threshold for the correlation coefficient of 0.6 was used as standard value of matching quality.

The results of the investigation are shown in figure 17. The comparison of these images shows that the matching with smaller sub-matrixes do not result in higher object details against matching based on standard 10x10 sub-window, however they do have strong noise. The smaller a sub-matrix is, the larger the achieved standard deviation is. When the directly neighbouring pixels are matched (row step =1, column step=1), the

corresponding sub-matrixes are overlapping by 90%, thus it gives not independent results. Moreover, the point spacing of just 1 pixel for matching extends the computation time significantly, although it leads to a slightly better shape. The image matching for every pixel has the disadvantage that the volume of data is bigger, that means the handling of the data is more difficult and takes more time. The results using this method are not better than in the case of three pixel point spacing. So a point spacing of three pixels has been used for matching – results see figure 17.

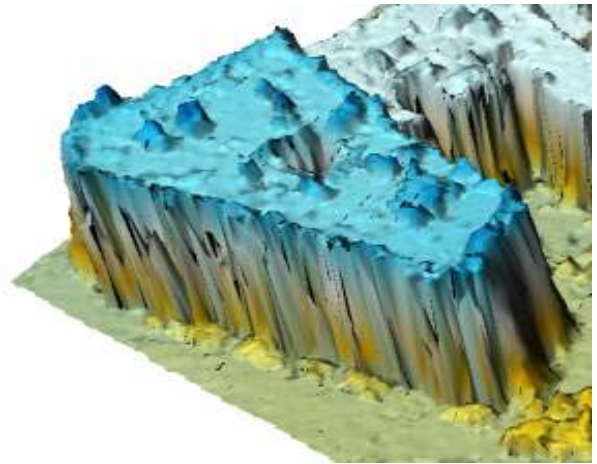
Based on the investigation for the next step the following parameters were used as defaults:

- window size 10 x 10
- maximum of iterations 10
- row step and column step 3
- correlation coefficient 0.6
- radiometric normalization Y
- region growing desired Y

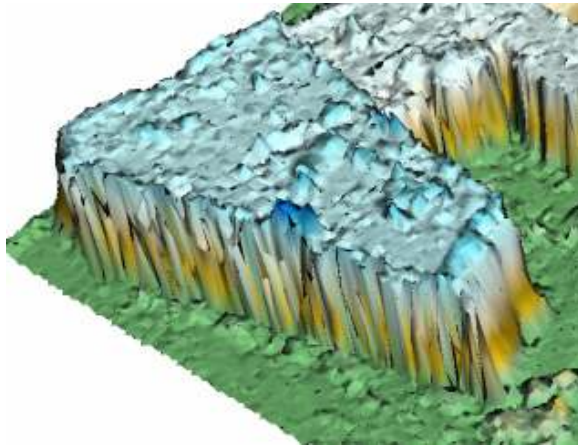
Since matching is made only in the specified in DPLX overview window, which is limited to 4000 x 4000 pixels, the processed areas were partitioned into the smaller overlapped sub-areas, usually with the size of 1600 x 1600 pixels. A sample report from DPCOR is attached in Appendix.



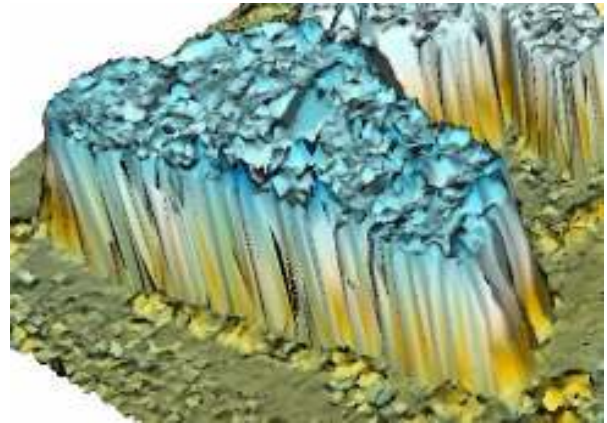
orthoimage



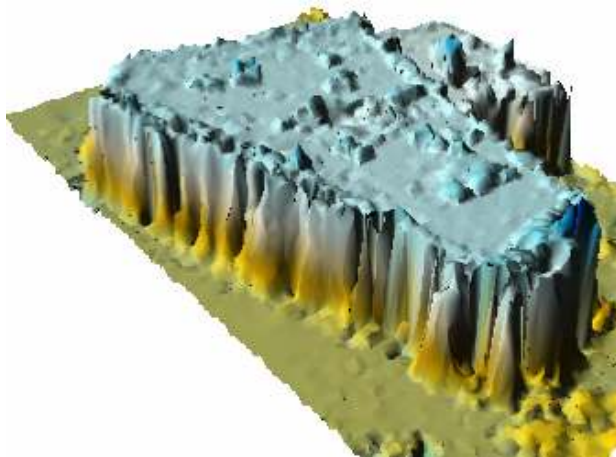
matrix 10x10, pixel spacing = 3



matrix 6x6, pixel spacing = 3



matrix 4x4, pixel spacing = 3



matrix 10x10, pixel spacing = 1

**Fig 17. Influence of initial parameters for DPCOR**

Additionally the matching accuracy was tested depending upon along-track overlap. Comparison investigations were carried out with 60% and 20% end lap. Results of the influence of the height to base relation are listed in the page 37. The size of the tested image matrix was 900 x 1800 pixels, it contains high building complexes typical for urban areas.

The standard deviation of the object height  $S_z$  is a linear relation of the average flying height above ground and the height to base relation.

$$S_z = \frac{h}{b} * S_{px} \quad (6) \text{ [Jacobsen, 2006]}$$

where:

$S_z$  – standard deviation of single point

$S_{px}$  – standard deviation of the x-parallax

$h$  – flying height above ground

$b$  – base (distance of used projection centres)

Since the flying height is fixed in the investigation, it is only possible for changing the height accuracy to change the base, which means the change of the overlap percentage. Table 4 shows the result. In order to estimate the standard deviation of the object height, a standard deviation of the x-parallax of 0.3 GSD was used [Jacobsen, 2005].

<b>Stereo pairs</b>	<b>covered [m]</b>	<b>end lap [%]</b>	<b>h [m]</b>	<b>base [m]</b>	<b>h/b</b>	<b><math>S_z</math> [m]</b>
<b>3051-3052</b>	642	69	1000	199	5.0	0.13
<b>3051-3053</b>	642	38	1000	400	2.5	0.07

**Table 3** Height to base relation for tested area and estimated height accuracy

where:

$h$  = flying height above ground

$S_z$  = estimated standard deviation of object height

Both data sets were matched by DPCOR with the above mentioned parameters. Stereo pair 3051-3052 has height to base relation of only 5.0. By simple theory, this is causing a poor vertical accuracy, but in the case of higher end lap the corresponding images are quite similar leading to a better matching (smaller value for  $S_{px}$ ). So the not so good height to base relation is compensated by the better image accuracy, with the advantage of a better view to the ground also in city areas. The following listed achieved results confirm this. The 20% overlap provides a larger angle of convergence, but at the same time increase the

area of occlusions. In stereo pair 3051-3052 over 30% points more matched correctly. Figure 18 shows the details.

### Stereo pair 3051-3052

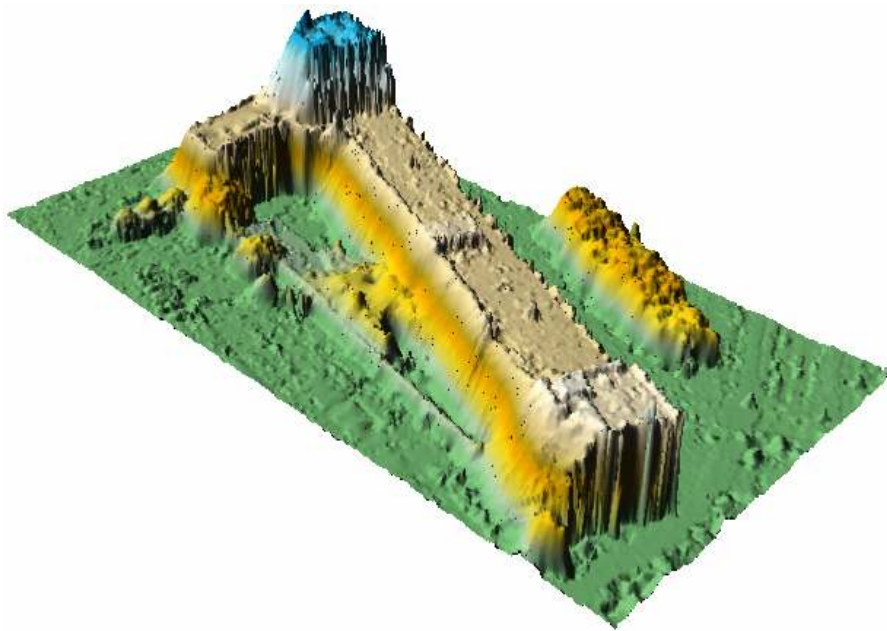
NUMBER OF FIRST SCENE	:	3051	
NUMBER OF SECOND SCENE	:	3052	
size of sub-image	:	1800	900
NO. OF SEED POINTS AVAILABLE	:	19	
NO. OF TRANSFER POINTS AVAILABLE	:	0	
TRANSFER PTS. OVERRIDDEN BY SEED PTS.	:	0	
NO. OF POINTS ATTEMPTED TO MATCH	:	180408	
NO. OF POINTS, THAT CONVERGED	:	169306	
NO. OF POINTS MATCHED CORRECTLY	:	145903	
NO. OF ERRORS (NO OR INCORRECT MATCH)	:	34505	
NO. OF POINTS NOT MATCHED	:	11102	
NO. OF SEED POINTS OUT OF SCENE 1	:	4	
NO. OF SEED POINTS OUT OF SCENE 2	:	0	
TRANSFER POINT OUT OF SCENE 2	:	0	
BOUNDARY PROBLEMS IN ADJ. ITERATIONS	:	152	
INITIAL VALUE OF RHO TOO SMALL	:	0	
SINGULARITY PROBLEMS IN ADJUSTMENT	:	0	
MAX. NUMBER OF ITERATIONS EXCEEDED	:	10946	

### Stereo pair 3051-3053

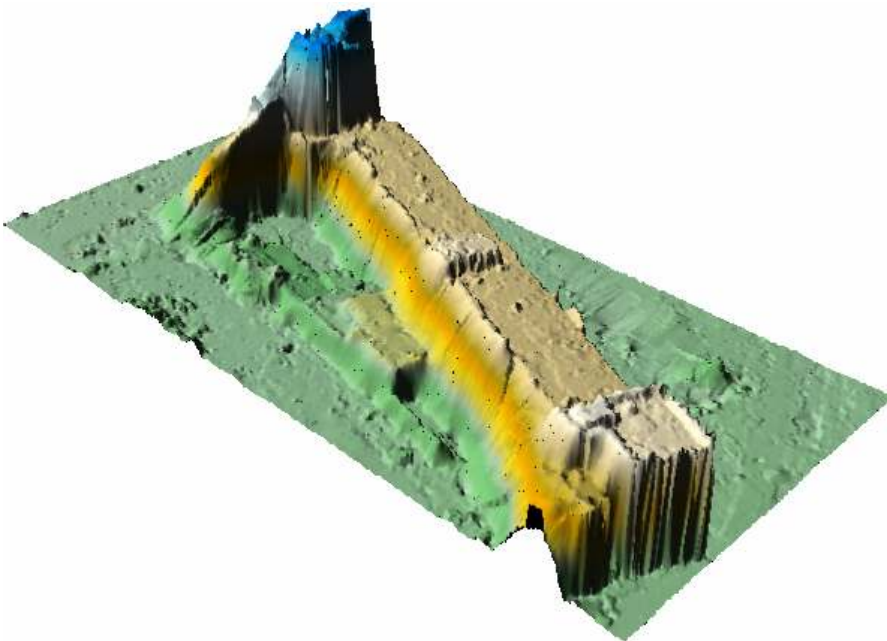
NUMBER OF FIRST SCENE	:	3051	
ROW, COL OF FIRST SCENE	:	1800	900
NUMBER OF SECOND SCENE	:	3053	
ROW, COL OF SECOND SCENE	:	1800	900
NO. OF SEED POINTS AVAILABLE	:	19	
NO. OF TRANSFER POINTS AVAILABLE	:	0	
TRANSFER PTS. OVERRIDDEN BY SEED PTS.	:	0	
NO. OF POINTS ATTEMPTED TO MATCH	:	127074	
NO. OF POINTS, THAT CONVERGED	:	119536	
NO. OF POINTS MATCHED CORRECTLY	:	101049	
NO. OF ERRORS (NO OR INCORRECT MATCH)	:	26025	
NO. OF POINTS NOT MATCHED	:	7538	
NO. OF SEED POINTS OUT OF SCENE 1	:	1	
NO. OF SEED POINTS OUT OF SCENE 2	:	0	
TRANSFER POINT OUT OF SCENE 2	:	0	
BOUNDARY PROBLEMS IN ADJ. ITERATIONS	:	74	
INITIAL VALUE OF RHO TOO SMALL	:	0	
SINGULARITY PROBLEMS IN ADJUSTMENT	:	0	
MAX. NUMBER OF ITERATIONS EXCEEDED	:	7463	



Test area



stereo pair  
3051-3052



stereo pair  
3051-3053

Fig 18. Image matching with different height to base relation

### 3.2.2. Computation of a ground coordinates – BLPRE → BLINT

The result of the image matching is a file containing corresponding pixels coordinates of the points, matched successfully. The ground coordinates of the matched points were computed by means of BLPRE and BLINT, belonging to program system BLUH.

Program BLPRE prepares non standard input data for the bundle block adjustment and can improve the image coordinates by different possibilities. It was used to calculate the image coordinates from pixel coordinates by affine transformation with the coefficients calculated from following UltraCam<sub>D</sub> camera parameters:

1	NUMBER OF PIXEL IN LINE	7500
2	NUMBER OF PIXEL IN COLUMN	11500
3	SIZE OF PIXEL IN LINE DIRECTION [MICRONS]	9.00
4	SIZE OF PIXEL IN COLUMN DIRECTION [MICRONS]	9.00
5	LOCATION OF ORIGIN 0 = UPPER LEFT	
10	FOCAL LENGTH [mm]	105.200

In BLINT object coordinates can be computed by intersection based on photo coordinates and the photo orientations. The coplanarity equation is applied. The exterior orientation was arranged as follows with sequence of rotation phi, omega, kappa.

	PHI	OMEGA	KAPPA	X0	Y0	Z0
3717	-.15931	.04325	.14739	6430133.106	5665883.647	1206.887
3718	-.19486	.02986	-.05349	6430333.022	5665882.000	1205.687
3719	-.18356	-.04914	-.28217	6430538.203	5665879.066	1205.226
3720	-.88922	-.56486	-.43224	6430739.300	5665876.237	1205.638

The result of the intersection is a file with XYZ ground coordinates of the matched points. The computed object coordinates for every sub-area were separately merged for the investigated areas ABN and MOP.

### 3.2.3. DSM analysis – DEMANAL

DEMANAL (analysis of digital elevation models) is a program that evaluates the accuracy and accuracy characteristics of a height model against a reference height model. The analysis of a DSM was made separately for distinct surface classes, e.g. buildings and ground, because the accuracy and the accuracy characteristics may be different depending upon the land cover. DEMANAL can use geocoded layer images for each land class. The program investigates in detail the discrepancies between both height models and also the dependency as function of the terrain inclination and the height level. It is possible to define tolerance limits for the terrain inclination and the discrepancies of the DSM-points. The influence of a vertical scale difference can be respected iteratively.

The software was used three times and both areas were processed the same manner. At first to evaluate the height data obtained straight from DPCOR image matching and then to determine the accuracy of the output DSM after interpolation and filtering with RASCOR and SURFER. Additionally DEMANAL was used for a comparative analysis of the generated 3D solids with the filtered DSMs.

Since no reference DSM was available for the investigated area, the generated product was compared to manual measurements. In order to assess the height data from automatic image matching, samples of the randomly-distributed points were measured by a human operator in the area of interest. Two separate sets of XYZ data were generated, for buildings and bare ground respectively. Table 4 shows the number of the measured points for each class. In this investigation the attention is focused on buildings as a main component of a city model, thus roof surfaces were covered densely with measurements in contrast to the terrain level. The MOP area had in general fewer points for comparison, because it contains less man-made objects than the ABN district.

<b>Class \ Area</b>	<b>ABN</b>	<b>MOP</b>
<b>Building points</b>	1584	663
<b>Terrain points</b>	350	276

**Table 4** Number of measured points

The used stereo model had the same orientation parameters as those used in BLINT for the intersection process. Hence the manual and automatic measurements are comparable. The analysis in DEMANAL was made in a single iteration, so without consideration of the vertical shift and the scale difference between both height data. Thus determined root-mean-square errors include random as well as systematic error components. Some measurements were not taken into account because of blunders. The maximal discrepancy between corresponding Z values was set to 10 meters. This threshold not only eliminates points of other classes from compared data sets but also indicates the less noisy data.

### **3.2.4. DSM interpolation and visualization – SURFER**

SURFER is a contouring and 3D surface mapping program that can convert scattered XYZ data into a grid arrangement for display and analysis. There are several methods of the grid data generation, among others Kriging, Nearest Neighbour, Natural Neighbour.

The *Triangulation with Linear Interpolation* method was used, which corresponds in SURFER to the Delaunay triangulation. The algorithm creates triangles by drawing lines between data points. The original points are connected in such a way that no point from the original data is inside the circum circle of any triangle, i.e. no triangle edges are intersected by other triangles. The result is a patchwork of triangular faces (TIN structure) over the extent of the grid. Then each triangle defines a plane over the grid nodes lying within the triangle, with the tilt and elevation of the triangle determined by the three original data points defining the triangle. All grid nodes within a given triangle are defined by the triangular surface. Because the original data are used to define the triangles, the height of the data points is computed by interpolation. Therefore, this method is an exact interpolator. However, in addition to sufficient matched points a number of not usable points like matched antennas, parts of chimneys, oblique surfaces like roof facets are included.

Using the option *3D Surface* a three-dimensional situation overview of the investigated area was obtained, in order to asset the results of every step.

Since the matching was done every third pixel, by theory it should be a nearly regular grid with 0.3 m spacing. In reality it was not, due to matching and occlusion problems. The data were interpolated to a grid format, i.e. a regularly spaced, a rectangular array of Z values from irregularly spaced XYZ data points was generated, by spatial interpolation.

On the one hand the grid data has to have the smallest cell size to describe the height discontinuities, but on the other hand the larger spacing provided less noisy data. A decision was made to generate two data sets for each area with spacing 0.6m and 0.9m respectively.

Moreover in the final step, the median filter was applied, i.e. the output grid node value equals the fifty percentile of the neighbouring values. In order to eliminate noise from roof surfaces, a matrix 3 x 3 was used in each case of DSM.

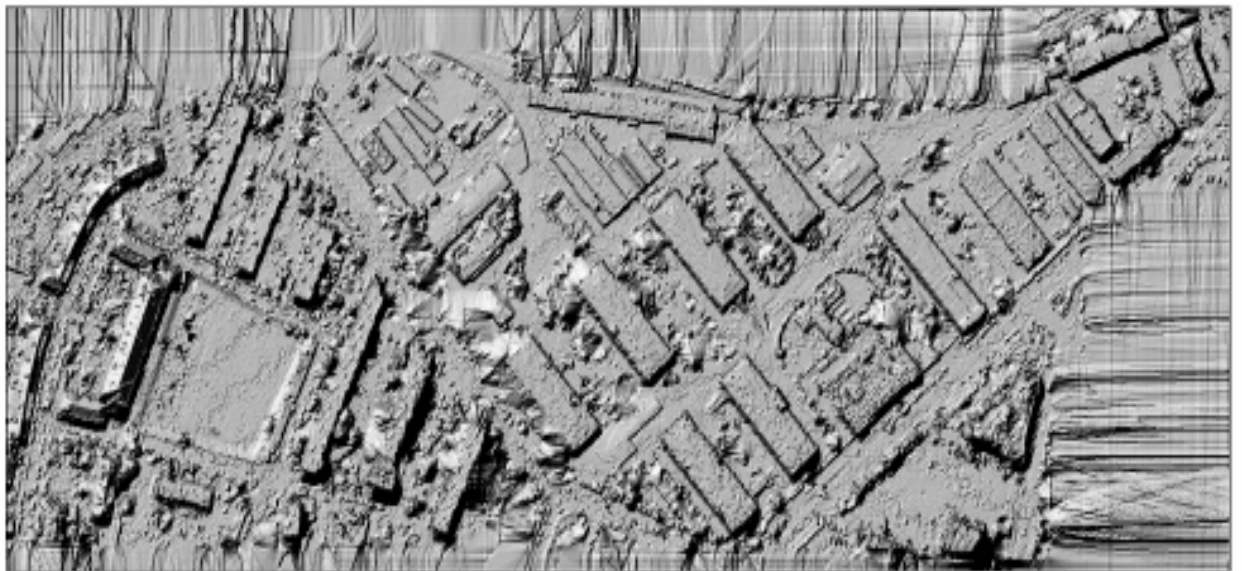


Fig 19. 3D surface (top) and shadow relief map (bottom) of MOP area in SURFER

### **3.2.5. DSM refinement – RASCOR**

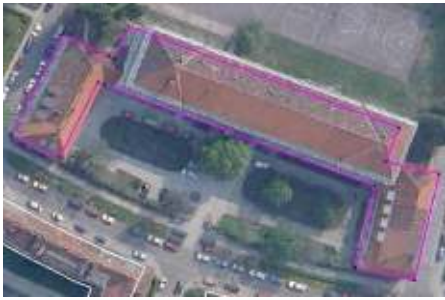
The program RASCOR (analysis, correction and plot of a height model) can analyze, improve, smooth and interpolate a digital elevation model which may be generated like by automatic image matching or laser scanning (LIDAR) in either an equal spacing or a random arrangement. RASCOR is eliminating the points which don't belong to the bare ground, generating a digital elevation model. It is using a sequence of different methods for the filtering of a DSM. The identification of points not located on the solid ground but on top of buildings or vegetation is possible by a minimal and maximal height in the area, by maximal height differences between neighbored points, by a sudden change of the height level, by a linear or polynomial interpolation in X- and Y-direction, by a minimal and maximal height difference against a local tilted plane or polynomial surface and a local prediction (least-squares interpolation) based on a tilted plane or polynomial surface. The final results can be filtered (smoothened) in relation to a rotated plane or polynomial surface fitted to the neighbored.

### **3.2.6. Building reconstruction – ATOP**

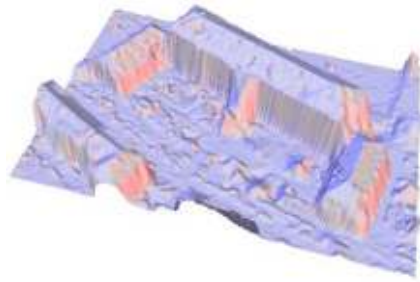
The main task of the study was the automatic reconstruction of buildings. The ATOP (Automated building reconstruction tool) software was used, which was developed by Claus Brenner at the University of Hanover, Institute of Cartography and Geoinformatic. ATOP is a program for the automated reconstruction of buildings from dense surface measurements, typically from laser scanning. However, the DSM from matching of aerial images was applied.

An initial data set for ATOP is a combination of a DSM in raster format and ground plans of buildings in vector format. Additionally the orthoimage is an input too. Although it doesn't affect the main reconstruction process, it supports the manual refinement as well as provides photorealistic texture of roof surfaces. Unfortunately in this investigation not a true orthoimage was available, therefore in some cases, especially in the case of high buildings, the texture doesn't correspond to building ground plans.

The following figures represent the steps of ATOP work flow.



Ground plans overlaid to orthoimage

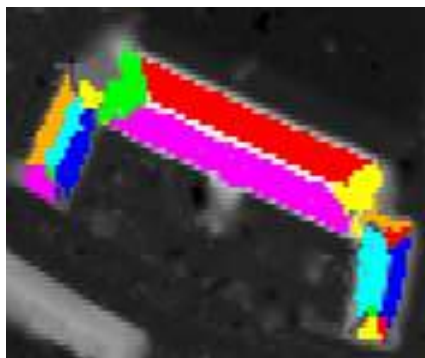


Digital Surface Model

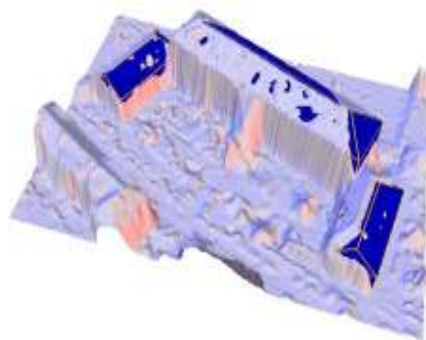
**Input data**



Portioned ground plan

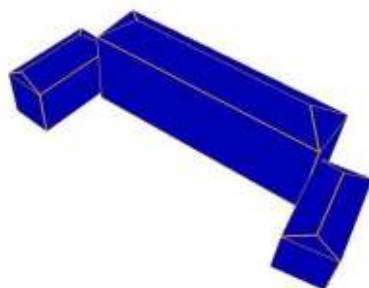


Segmented DSM data



Adjusted primitives

**Processing**



Output solids

**Output**

**Fig 20. ATOP processing**

The process starts by decomposing the building outline polygon into two-dimensional primitives (rectangles), which is done by a heuristic algorithm analyzing given GIS data. Each two-dimensional primitive is the footprint of a corresponding three-dimensional primitive. Thus, the first three parameters of the primitive are estimated, namely height and width (extension of the rectangle) and orientation (horizontal rotation). The parameters of the roof, i.e. roof type (from a fixed library), height of the eaves and roof slope are determined using segmentation and the least-squares adjustment. The DSM data in a raster format is segmented into planar surface by an analysis of every pixel's gradient. Since the direct computation of a normal vector tends to amplify noise, a local least-squares adjustment is determined within small matrix around each element of the DSM. The region growing method covers pixel by pixel the whole primitive footprint with segmented planes. Although the segmentation into normal vector compatibility regions describes roof structure quite well, the choice of seed pixel of a region strongly affects the results. In the next step ATOP adjust each primitive from the fixed library, with already estimated 2D parameters, to the planar surfaces by the least-squares method. The minimal score of the adjustment process points the remaining 3D parameters of the right primitive, which are height of a solid, roof type and roof slope.



**Fig 21. Primitive types in ATOP**

Six roof types are embedded in the tested version of ATOP. There are: flat roof (one horizontal face), ridge roof (two sloped faces), hipped roof (three or four sloped faces), desk roof (one sloped face), cone roof (cylinder with cone tip), ellipse roof (extruded ellipse with ellipsoid on top). With flat roofs, the parameter “ridge” has no effect. Ridge, hipped and desk roof carry an orientation. With ridge roof, this is one of the two possible ridge orientations. With hipped roofs consisting only of 3 slanted surfaces, it is the number of the gable end, with desk roofs it is the number of the lower horizontal eave edges. The orientation can be chosen with the arrow buttons. Cone roof and ellipse roof do not have rectangular ground plans. Cone roof uses a rounded rectangle and ellipse roof an ellipse inscribed into the rectangle. The 2D view always shows a rectangle. Cone roof is a cone on top of a cylinder if the 2D projection is a square. Ellipse roof is an ellipsoid on top of an extruded ellipse.

The automatic reconstructed solids can be refined by adding other primitives or changing all six estimated parameters. In order to support user edition, during manual adjustment of the primitives the global RMS is computed online. The final version of singles cuboids is exported either in DXF or VRML format, to merge them into buildings and visualize entire scene.

The both areas ABN and MOP were tested twice by ATOP software, once with object point spacing 0.6m and second time with 0.9m. In every case neither cone roof nor ellipse roof was taken under consideration.

### 3.3. Results

#### 3.3.1. Generation of DSM

Since digital surface model of MOP area as well as of ABN was generated from the sub-images with approximately 1600 x 1600 pixels, it is not easy to evaluate the overall image matching process. Every matrix had different combination of land cover components, thus different matching conditions. However, comparing the total number of computed ground points with the extension of the corresponding image grid, the percentage of correctly matched points can be estimated. The numbers are shown in Table 5.

ABN	number of columns	number of rows	attempted to be matched	correctly matched	percentage
1 pixel spacing	3387	9013	-	-	
3 pixels spacing	1129	3004	3 391639	2 683 991	79%

MOP	number of columns	number of rows	attempted to be matched	correctly matched	percentage
1 pixel spacing	9264	3814	-	-	
3 pixels spacing	3088	1271	3 926 123	2 567 688	65%

**Table 5. Overall correctly matched points**

In both cases nearly over 60% of the possible points were matched with correlation coefficient exceeding 0.6. So for 30% of the points matching was either not satisfying or impossible. Although, the results for MOP area are considerable lower, this does not affect buildings, because in this area lots of trees can be found, where the matching failed.

The output of DPCOR's computation is satisfying and does not differ from expectation. This moderate result can be explained by means of figure 22. The sample of image 3717 shows the overlapping matrixes with the correctly matched points and the matching gaps. They are caused by common problems of the automatic DSM generation from aerial images in urban area, in particular forest areas, occlusions, shadows or poor texture. The difficulties are rather independent upon the image matching procedure and sometimes it is impossible even for a human operator to find conjugate positions.

In the most of cases the matching failed because of poor texture in the shadow areas and due to occlusions, i.e. lack of correspondence point in the other image.

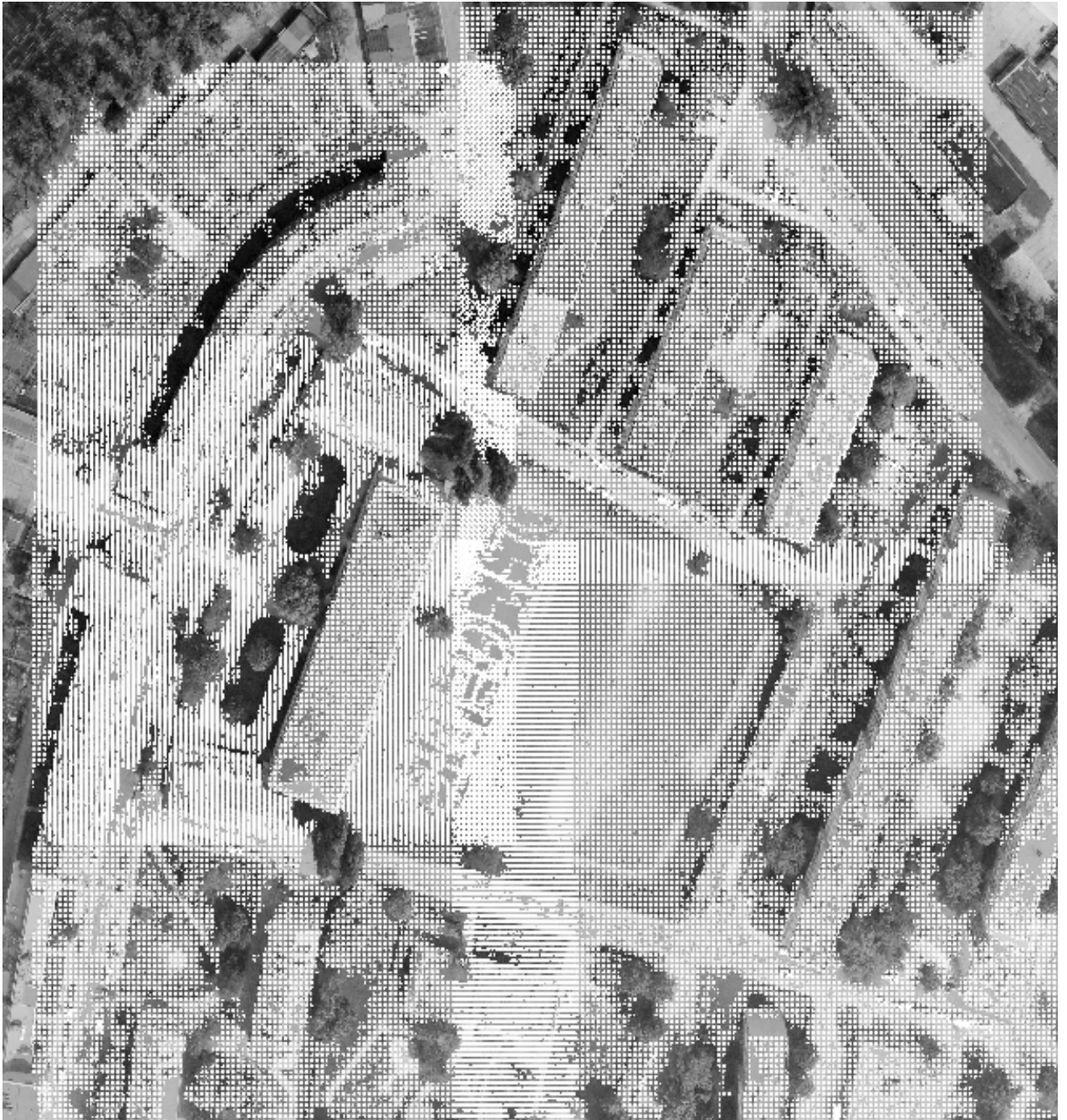


**Fig 22. Overlay of matched points in image 3717**

The example of the shadow can be seen in the upper left corner, caused by the C-shaped building. Moreover in more dense-building district ABN the objects often occlude each other, which also disturb the matching process. Man-made objects with smooth or sleek surface, e.g. industrial plants, may have also poor texture, disturbing the matching. One of the biggest

difficulties for matching are forest areas. The trees occur randomly over the study area, which results in typical round spots without ground points. And even if they are matched partially, the points usually cause noise over the area rather than provide good tree structure.

Nevertheless the interesting areas, namely roof surfaces, had sufficient texture information and in general were covered completely with the correct points. However, the roof infrastructure like antennas, air condition units and chimneys cause the distinct roof surface discontinuity. Majority of the mentioned matching problems can be handled partially with a good interpolation and filtering procedure.

In order to evaluate the refinement step, the results obtained in both cases, raw and improved DSM, were analyzed. A comparative study regarding the accuracy of the DSM generated with and without interpolation and filtering is presented below. The analyzed test areas are ABN and MOP and the analysis was made separately for roof surfaces and terrain level.

## ABN

The generation and analysis of the DSM for ABN area was made with three variations of the height data. For every height data set the Root-Mean-Square Error (RMSZ) was calculated. At first for raw data, i.e. randomly distributed ground points derived directly from the image matching process, secondly using two iterations with RASCOR, interpolation and median filtering in SURFER, in 0.6m and 0.9m grid spacing arrangement. The urban area ABN has a broad diversity of the terrain features, including many types of the building roofs. The achieved results are presented in table 6 and in figure 23. Additionally the frequency distributions of the discrepancies between generated DSMs and reference measurements are shown in figure 24, for buildings and bare terrain respectively.

DSM	Class	RMSZ [m]	Mean DZ [m]	RMSZ without bias [m]
Raw	Buildings	0,59	0,26	0,53
	Terrain	0,44	0,13	0,42
Grid 0.6 m	Buildings	0,61	0,45	0,41
	Terrain	0,36	0,00	0,36
Grid 0.9 m	Buildings	0,58	0,21	0,54
	Terrain	0,29	0,00	0,29

**Table 6. DSM accuracy results for test area ABN**

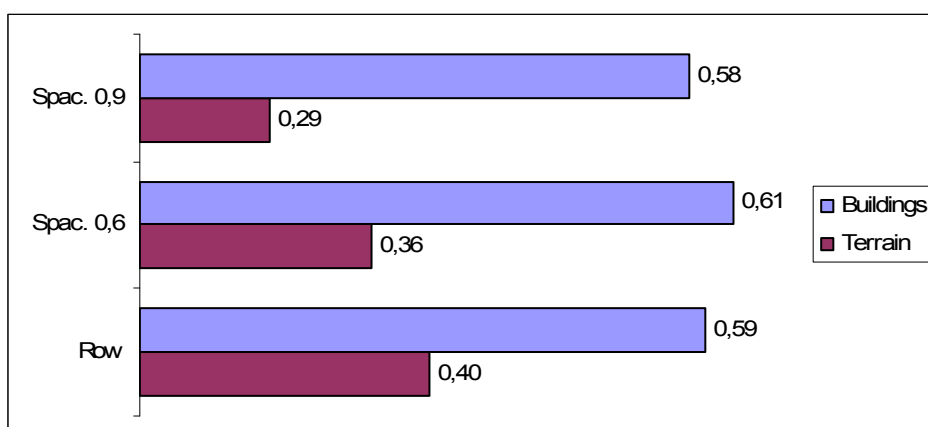


**Fig 23. RMSZ for DSM variations of ABN area**

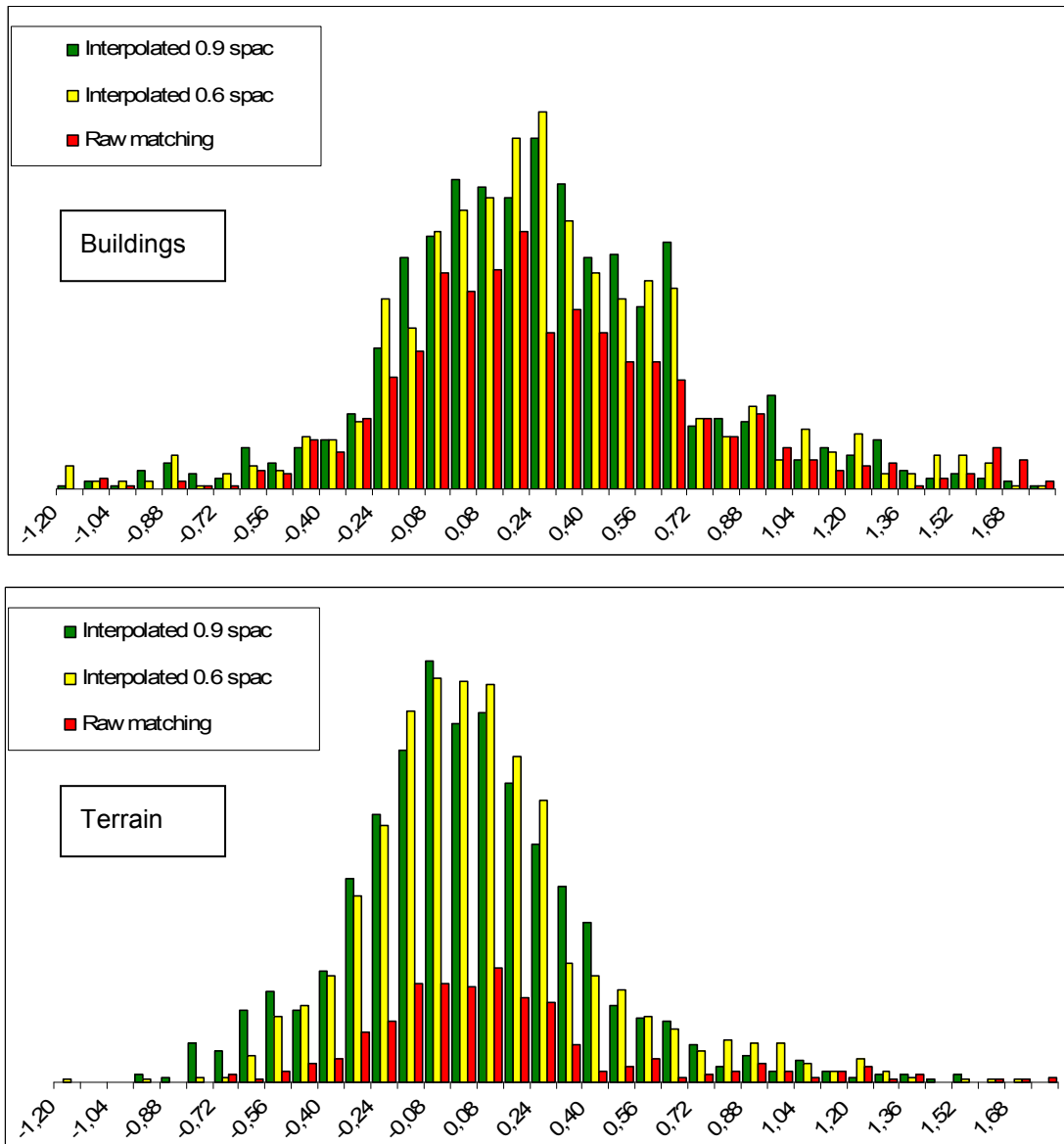


**Fig 24. Frequency distribution of discrepancies DZ**

According to Figure 23 the terrain class has nearly 50% smaller RMSZ than the building class in the every variation of the DSM. The terrain in Wroclaw has a rather homogenous flat character, thus it is easier to reconstruct its surface in a comparison with variety of building structure. Moreover, the interpolation and filtering gives immediately better results in the ground surface, which is reflected in Figure 24 (bottom), only few ground points were taken into analysis of the raw DSM, compared with interpolated data. In the case of buildings the RMSZ is almost the same for each data set. The frequency distribution of discrepancies for the building class shows small influence of the interpolation on the amount of blunders, i.e. nearly the same number of the reference points taken into account.

## MOP

The DSM for MOP area was generated and analyzed exactly in the same manner as the previous area of interest. Since MOP is a part of suburban district, it contains mostly simple industrial buildings and well distributed residential blocks. The obtained results for one data set with ground points straight from automatic image matching, and two sets with reduced data to a grid arrangement are shown in Table 7 and in Figure 25. The frequency distributions are shown in figure 26.

DSM	Class	RMSZ [m]	Mean DZ [m]	RMSZ without bias [m]
Raw	Buildings	0,42	0,16	0,39
	Terrain	0,39	0,19	0,34
Grid 0.6 m	Buildings	0,41	0,03	0,41
	Terrain	0,38	0,12	0,37
Grid 0.9 m	Buildings	0,39	0,04	0,39
	Terrain	0,35	0,07	0,34

**Table 7. DSM accuracy results for test area MOP**

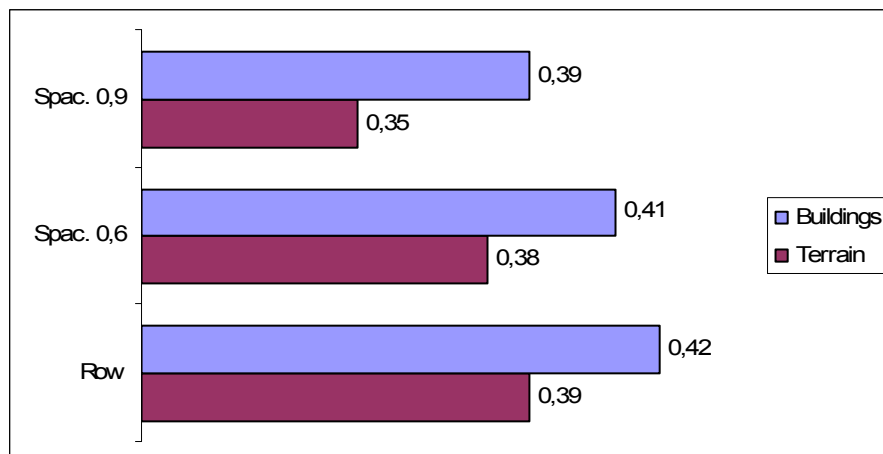


**Fig 25. RMSZ for DSM variations of MOP area**

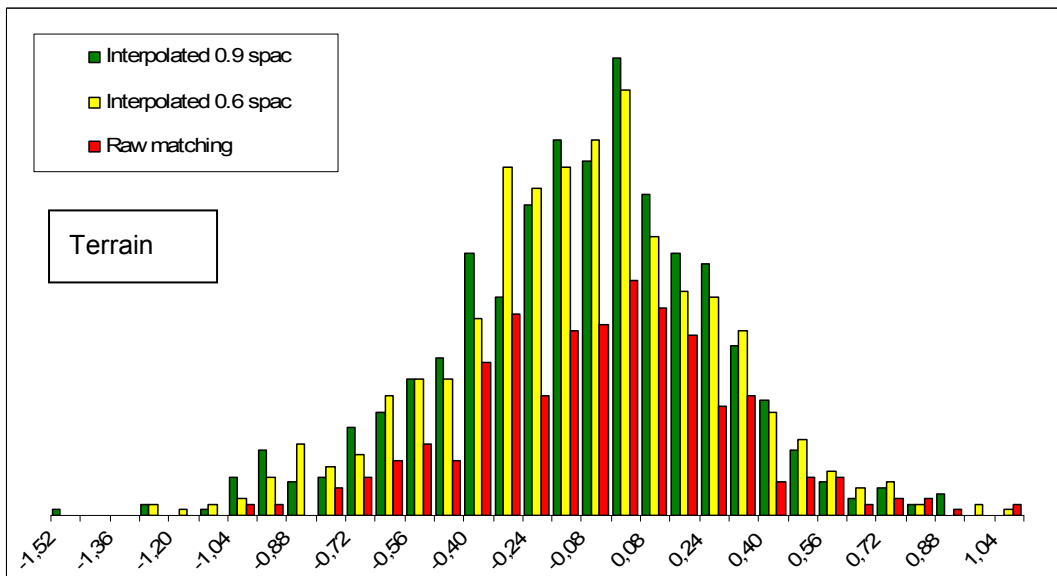
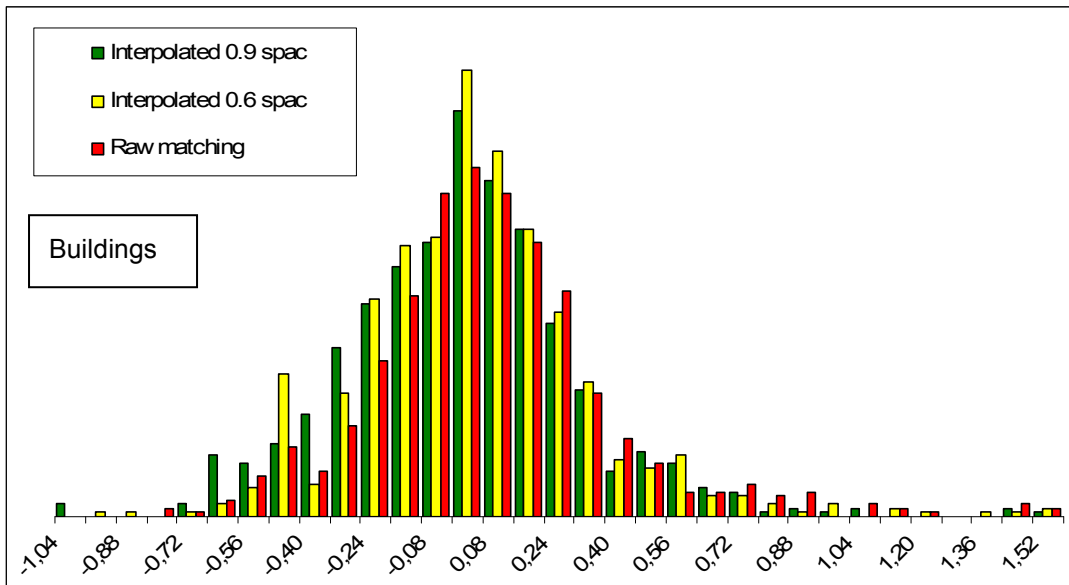


**Fig 26. Frequency distribution of discrepancies DZ as F(DZ)**

Similar to ABN area the blunders and random discrepancies can be fast eliminated by interpolation and filtering in the terrain-points class. Also the RMSZ of this land cover class is smaller than for buildings, however, not as much as in previous case. Furthermore Figure 25 shows that the larger grid spacing results in smaller RMSZ for both classes.

In every variation of the generated DSM for MOP area, the value of RMSZ was smaller than in ABN case and also the frequency distributions are more symmetric in the case of suburban area. Since the buildings are well-spaced and their roof structures are not complex, there is no large difference in accuracy between these data sets.

### 3.3.2. Building reconstruction

For both study areas the buildings were reconstructed based on two data sets, namely DSM grids with pixel spacing 0.6m and 0.9m respectively. No ground truth is available for any of the data sets. Therefore, the generated building models can be verified only by visual inspection, which showed that more than 70% for ABN and 80% for MOP area outlines gave correct reconstruction, i.e. the reconstructed shape is true to reality except tolerated omissions of small details such as dormers or chimneys. The main failures are due to wrong partition process, meaning partition results had either false arrangement within footprint or were too small to perform primitive fitting. Some examples of false reconstruction are shown in figure 27.

Because of missing ground truth, the verification of the accuracy of the reconstructed models is rather problematic. The global Root Mean Square Error was calculated by comparison between initial DSMs and pseudo DSMs generated based on vector data derived from reconstructed solids. Over 150 000 points were taken into account. The situation plots of compared data are presented in figures 28 and 29, where grey values stands for:

```

NO REFERENCE HEIGHT AVAILABLE          0
REFERENCE HEIGHT, BUT OUTSIDE LAYER    80
USUAL HEIGHT POINT INSIDE LAYER       170
EXCLUDED - EXCEEDING Z-TOLERANCE      255
EXCLUDED - EXCEEDING SLOPE-TOLERANCE   40

```

The Z tolerance was fixed to 10 m, in order to avoid comparison between ground points. The white spots over building areas indicate either lack of reconstruction or wrong choice of the primitive. Table 8 shows general results for both study area.

Area	DSM spacing [m]	Number of outlines	Number of primitives	Correct reconstruction	RMSE [m]
ABN	0.6	147	127	73%	1.74
	0.9		146	78%	1.81
MOP	0.6	60	52	86%	1.12
	0.9		58	96%	1.09

**Table 8. Accuracy of the generated building models**

Two types of failure can be stated: wrong partition process and wrong fitting results. Naturally these mistakes are connected with each other; usually wrong partition causes the

wrong choice of primitive. However, sometimes the adjustment process results in the incorrect roof type because of the image matching problems, which was mentioned before. Even though the external data source was used, namely building outlines, it can be easily noticed that not every object was reconstructed. Despite the fact that some of the buildings consist of more than just one primitive, the overall number of the primitives is smaller than the number of the initial ground plans.

Of course, the reconstruction results are better for suburban than for dense built-up areas. Generally in MOP area more buildings had correct representation in CSG solids, which also reflects in the smaller value of RMSE. It can be said that in the suburban part all reconstructed buildings were correctly represented. Problems appear at the fitting of small primitives, and that is why few of buildings were not reconstructed.

In contrast to MOP area, where most roof structures were gable or flat, the ABN structures were more complex and irregular. Despite this, ATOP handled it better than expected, the solid's reconstruction results were satisfying in nearly 80% of the cases. However, in 20% of the outlines the generalization is too strong or algorithm did not determine any primitive. Additionally the matching failed more often in this area, due to number of occlusions caused by trees and adjacent buildings, which also reduced the reconstruction reliability.

Even though the 0.6m grid data better preserve steep edges and surface discontinuity, in both areas automatic process performed better with 0.9m spacing. And it regards not only the correctness of the building representation as combination of solids, but also the reconstruction process in general. In many cases, using DSM with 0.6m spacing, algorithm either did not reconstruct small parts of the building or did reconstruct but regardless of the outline complexity (see figure 27).

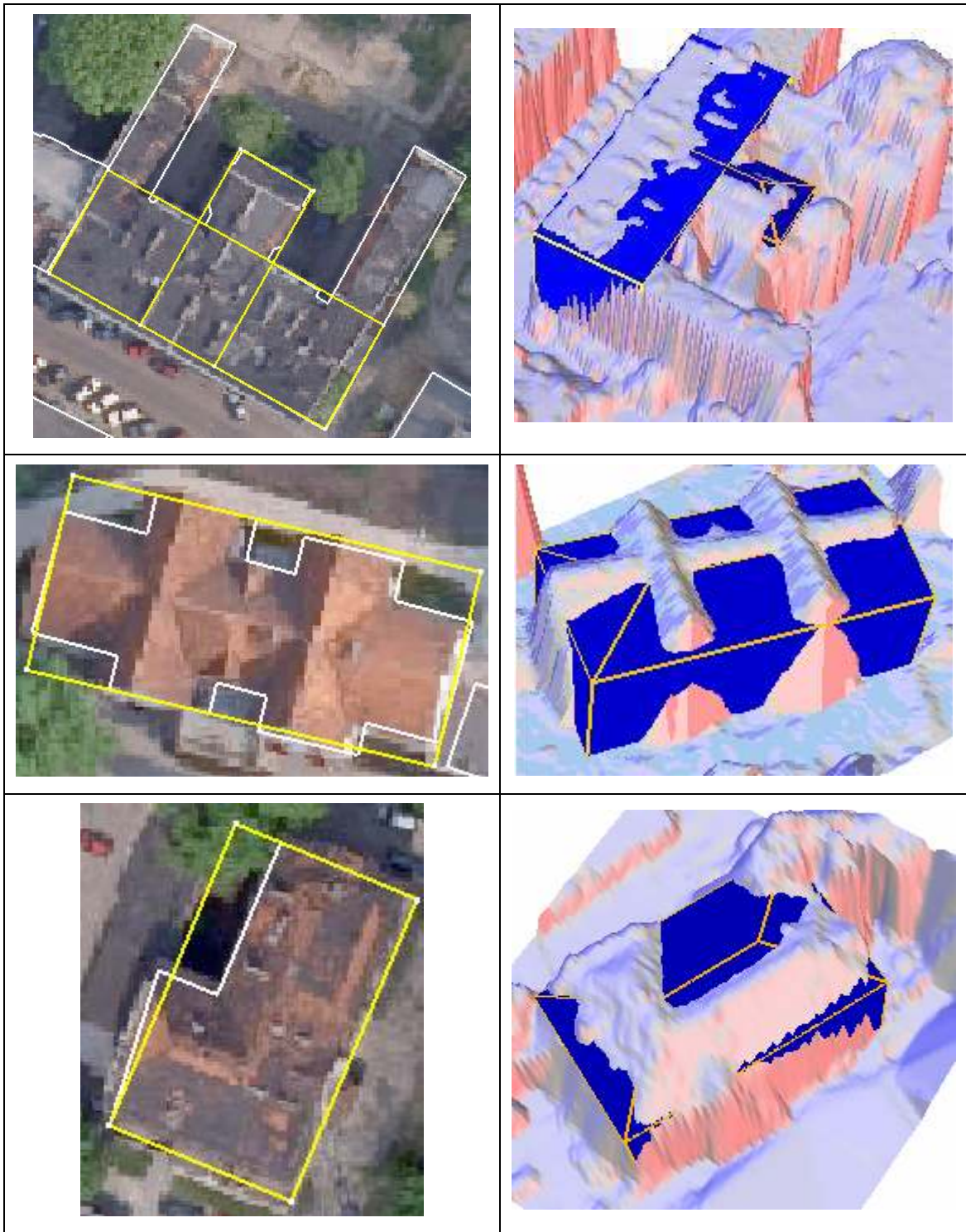
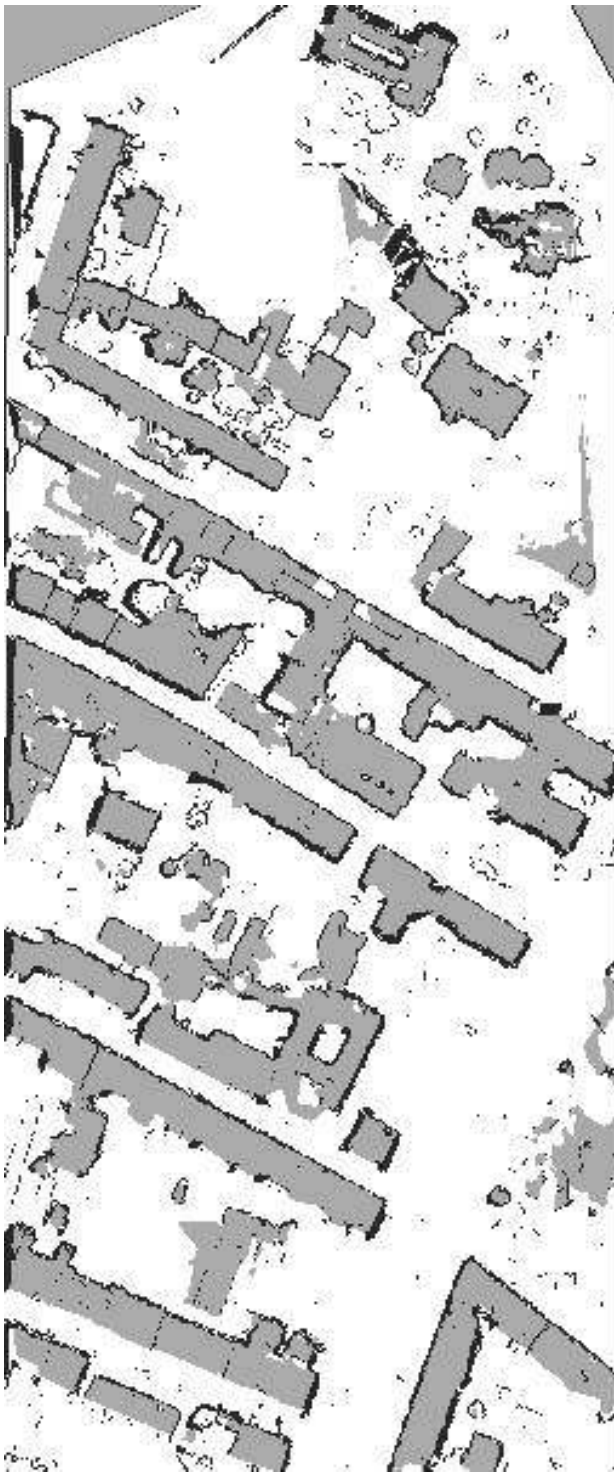
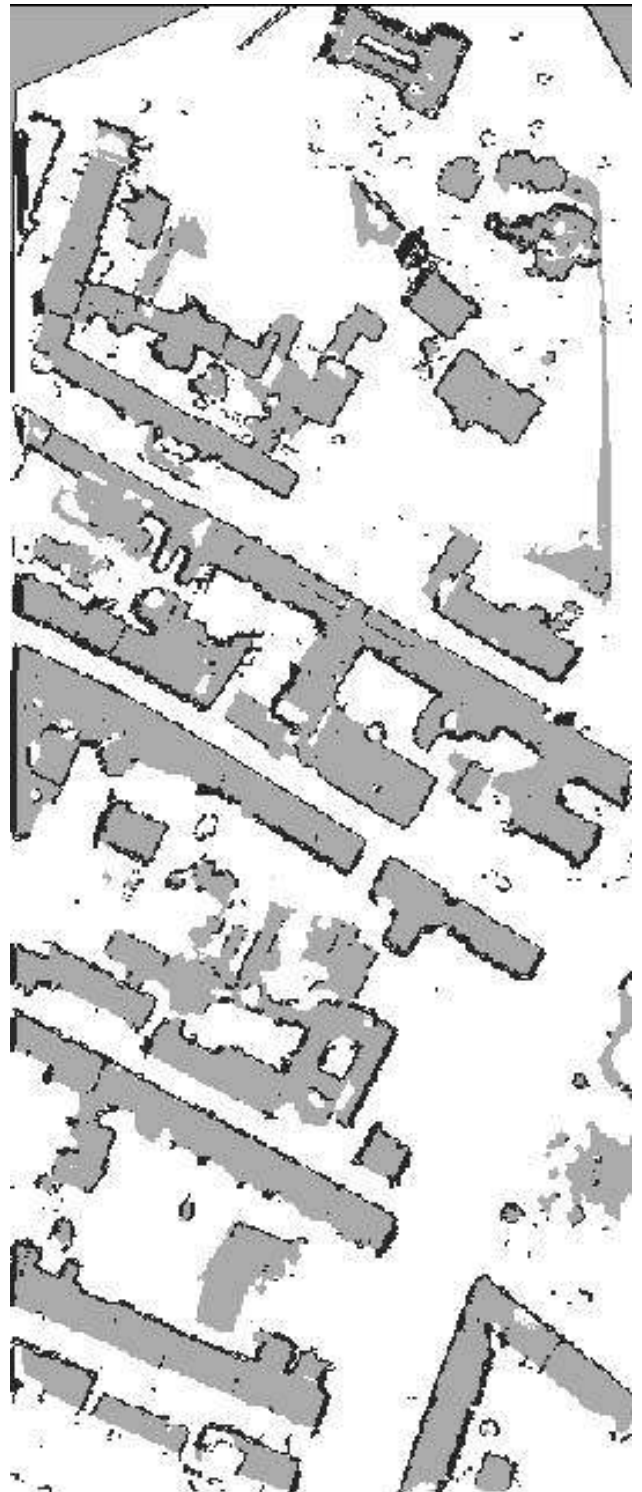


Fig 27. Errors in reconstruction

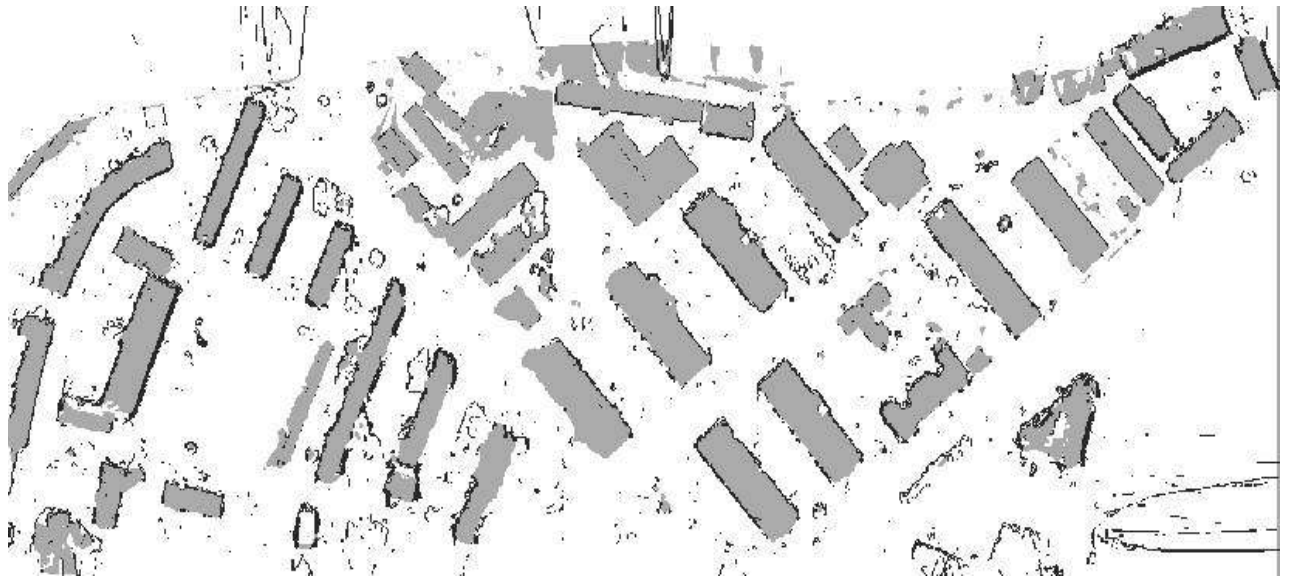


ABN 0.6 m

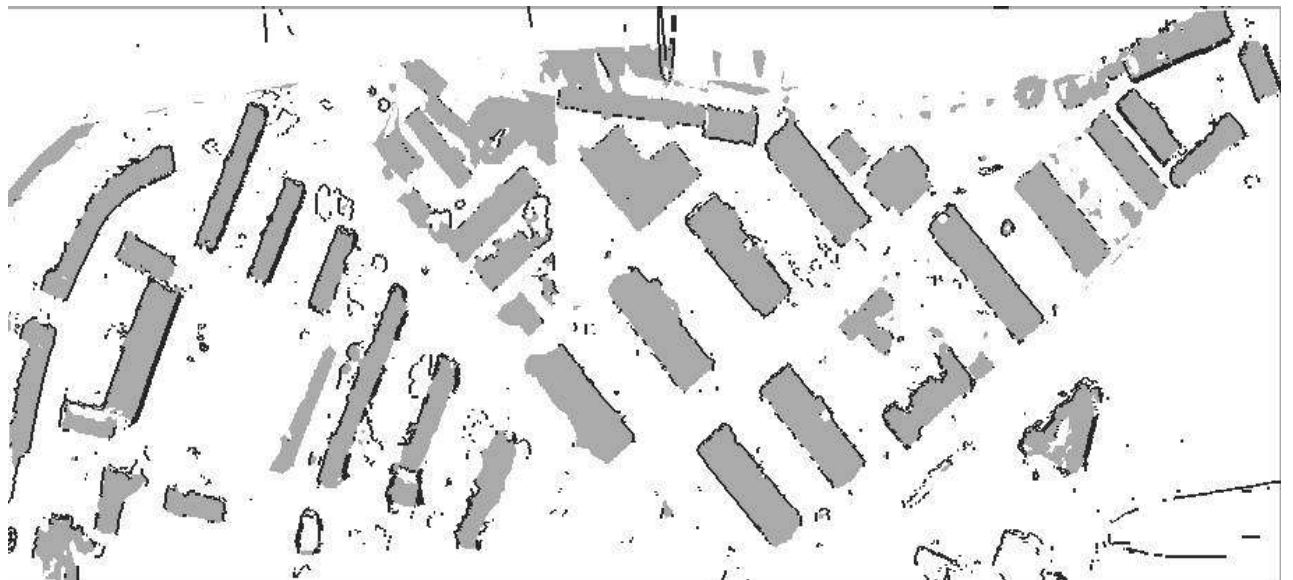


ABN 0.9 m

Fig 28. DEMANAL situation plots for pseudo DSMs – ABN area



MOP 0.6 m



MOP 0.9 m

Fig 29. DEMANAL situation plots for pseudo DSMs – MOP area

## 4. CONCLUSION

3D-City models are becoming more and more competitive to two-dimensional geographic information systems. Various data sources, including ground surveys, aerial images and airborne laser scanning were analyzed for the purpose of automatic 3D-city model generation. Up to now no fully automatic commercial systems are available, although promising results have been stated in several investigations.

Although, the trend of current studies definitively shows decreasing part of aerial images in automatic 3D data acquisition in relation to ALS systems, the presented investigation was focused on digital imagery as a data source for 3D city modelling.

The analysis of the digital surface model obtained from high-resolution-aerial images was made as well as its usefulness was assessed with respect to automatic generation of three-dimensional city models. Two areas have been investigated, namely a suburban and densely built-up area. The Program System BLUH was used for the generation of DSMs and to evaluate its accuracy. Furthermore the building reconstruction process based on image-derived height data was tested in ATOP software.

Digital surface models were generated by the least-squares image matching, which is based on the region-growing algorithm in program DPCOR with a point spacing of 3 pixels and a threshold for the correlation coefficient of 0.6. Optimal values of the matching have been determined by a comparative analysis of the tests results carried out with image samples of 1600 x 1600 pixels. Additionally the influence of the height to base relation to the accuracy and quality of the generated DSM was investigated. Even though the matching of images with 30% end lap had resulted with higher vertical accuracy, the height data were obtained from 60% end lap image combinations in regard to their better quality, i.e. higher number of correct matched points. The matching in suburban scene was significantly worse due to problem with trees for matching, which did not influence quality of buildings.

The data acquired from automatic image matching is not in a regular arrangement and it usually contains gaps in the parts of the image that could not be matched or were matched incorrectly. In order to overcome these drawbacks an interpolation was applied and the grid-arrangement height data with spacing of 0.6m and 0.9m was generated. The overall RMSZ was calculated for each area with a random and grid distribution. There is significant difference between the terrain and the building part of the scene. Comparison with manual stereo measurements proved that the interpolation refines the DSM over terrain level (streets, bare ground) but in general does not improve the results over buildings. Only blunders can be removed with its help.

Two variations of DSM grids for both test area were used in order to reconstruct building geometry by program ATOP. Additionally the GIS database containing planar outlines of buildings was employed as external data source. With this data set over 70% of buildings in urban area and 80% in suburban district were reconstructed. Accuracy of the model generated from 0.6m and 0.9m grid is in the same level, while quality is considerably better in the case of DSMs with a spacing of 0.9m. In every presented statistic the suburban area shows better results because of its building simplicity. The quality of generated models is between LoD 1 and LoD 2 according to CityGML classification.

## **ACKNOWLEDGEMENTS**

I would like to thank and acknowledge the help and advice of Dr.–Ing. Karsten Jacobsen from the Institute of Photogrammetry and Geoinformation (IPI), Leibniz University of Hannover. I would also like to thank Dr.–Ing. Ryszard Preuss from the Faculty of Geodesy and Cartography, Warsaw University of Technology and Dipl.–Ing. Claus Brenner from The Institute of Cartography and Geoinformatics, Leibniz University of Hannover for the support during the project period and all the advice they gave me.

# APPENDIX

---

## Sample report from DPCOR

---

CONTROL FILE: C:/Od\_Marcina/mgr/3717\_3720/test.prj  
LOG-File : C:\Od\_Marcina\mgr\3717\_3720\test.log  
TITLE : Title  
SUBTITLE : Suptitle  
CODE OF MATCHING : 1  
NAME OF FIRST SCENE: C:\Od\_Marcina\mgr\3717\_3720\3717\_pan.kcl  
NUMBER OF FIRST SCENE : 3717  
SCENE ORIENTATION (DEGREES.DECIMALS): 0.000  
ANGLE OF INCIDENCE (DEGREES.DECIMALS): 0.000  
ROW, COL OF FIRST SCENE : 1600 1600  
UPPER LEFT CORNER OF FIRST SCENE : 9287 3000  
NAME OF SECOND SCENE : C:\Od\_Marcina\mgr\3717\_3720\3718\_pan.kcl  
NUMBER OF SECOND SCENE : 3718  
SCENE ORIENTATION (DEGREES.DECIMALS): 0.000  
ANGLE OF INCIDENCE (DEGREES.DECIMALS): 0.000  
ROW, COL OF SECOND SCENE : 1600 1600  
UPPER LEFT CORNER OF SECOND SCENE : 9250 875  
SCALE PARAMETER IN X AND STAND. DEV. : 1.0000 0.0000  
SHEAR PARAMETER IN X AND STAND. DEV. : 0.0000 999999984306749440.00  
SCALE PARAMETER IN Y AND STAND. DEV. : 1.0000 0.0000  
SHEAR PARAMETER IN Y AND STAND. DEV. : 0.0000 999999984306749440.00  
FILE WITH CONJUGATE POINTS (INPUT) : N  
FILE WITH MATCHED CONJUGATE POINTS : C:\Od\_Marcina\mgr\3717\_3720\conj.out  
FILE WITH MATCHED DTM POINTS : C:\Od\_Marcina\mgr\3717\_3720\m3.pix  
ACTUAL WINDOW SIZE : 10  
MAX. NUMBER OF ITERATIONS : 10  
ROWSTEP, COLSTEP : 3 3  
PERCENTAGE FOR RADIOM. NORMALIZATION : 10.000  
SHIFT BOUND FOR CHANGES OF UNKNOWNNS : 0.050  
SCALE BOUND FOR CHANGES OF UNKNOWNNS : 0.010  
SHEAR BOUND FOR CHANGES OF UNKNOWNNS : 0.010  
ACCEPTANCE BOUND CORREL. COEF. : 0.600  
ACCEPTANCE BOUND FOR ERROR ELLIPSE : 5.000  
MAX. DIFFERENCE TO INITIAL VALUES : 20.000  
UPPER BOUND FOR CORREL. COEFF. : 1.100  
MIN / MAX BOUND FOR SCALE-PARA. A1 : 0.3000 3.0000  
MIN / MAX BOUND FOR SCALE-PARA. B2 : 0.3000 3.0000  
MIN / MAX BOUND FOR SHEARE-PARA. A2 : -1.0000 1.0000  
MIN / MAX BOUND FOR SHEARE-PARA. B1 : -1.0000 1.0000  
RADIOMETRIC NORMALIZATION (Y/N) : Y  
REGION GROWING DESIRED (Y/N) : Y  
TRANSFER POINTS AVAILABLE (Y/N) : N  
AFFINPAR. (Y/N) :

CURRENT DATE : 13.04.2007  
CURRENT TIME : 08:39:15



SINGULARITY PROBLEMS IN ADJUSTMENT	:	10
MAX. NUMBER OF ITERATIONS EXCEEDED	:	8323
NO. OF POINTS MATCHED INCORRECTLY	:	27208
ERROR 1: RHO TOO SMALL	:	25659
ERROR 2: AX OF ERROR ELLIPSE TOO LARGE	:	0
ERROR 3: DIFF. TO INIIAL VAL. TOO LARGE:	:	0
ERROR 4: A1 TOO SMALL	:	0
ERROR 5: A1 TOO LARGE	:	0
ERROR 6: B2 TOO SMALL	:	1687
ERROR 7: B2 TOO LARGE	:	1
ERROR 8: A2 TOO SMALL	:	203
ERROR 9: A2 TOO LARGE	:	257
ERROR10: B1 TOO SMALL	:	0
ERROR11: B1 TOO LARGE	:	0
ERROR 1 ONLY	:	25659
ERROR 2 ONLY	:	0
ERROR 3 ONLY	:	0
ERROR 1 AND 2	:	0
ERROR 1 AND 3	:	0
ERROR 2 AND 3	:	0
ERROR 1, 2 AND 3	:	0

HISTOGRAMS OF ALL CORRECTLY MATCHED POINTS

-----

NUMBER OF POINTS IN EACH HISTOGRAM	:	219840
CORRELATION COEFFICIENT		
NO. OF POINTS WITH RHO > 0.95	:	81403
NO. OF POINTS WITH 0.90 < RHO < 0.95	:	45847
NO. OF POINTS WITH 0.85 < RHO < 0.90	:	30526
NO. OF POINTS WITH 0.80 < RHO < 0.85	:	20902
NO. OF POINTS WITH 0.75 < RHO < 0.80	:	14413
NO. OF POINTS WITH 0.70 < RHO < 0.75	:	10873
NO. OF POINTS WITH 0.65 < RHO < 0.70	:	8691
NO. OF POINTS WITH 0.60 < RHO < 0.65	:	7185
NO. OF POINTS WITH 0.55 < RHO < 0.60	:	0
NO. OF POINTS WITH 0.50 < RHO < 0.55	:	0
NO. OF POINTS WITH 0.45 < RHO < 0.50	:	0
NO. OF POINTS WITH 0.40 < RHO < 0.45	:	0
NO. OF POINTS WITH 0.35 < RHO < 0.40	:	0
NO. OF POINTS WITH 0.30 < RHO < 0.35	:	0
NO. OF POINTS WITH 0.25 < RHO < 0.30	:	0
NO. OF POINTS WITH 0.20 < RHO < 0.25	:	0
NO. OF POINTS WITH 0.15 < RHO < 0.20	:	0
NO. OF POINTS WITH 0.10 < RHO < 0.15	:	0
NO. OF POINTS WITH 0.05 < RHO < 0.10	:	0
NO. OF POINTS WITH 0.00 < RHO < 0.05	:	0
NO. OF POINTS WITH RHO < 0.00	:	0

---

## Matching Data Statistics Report for ABN Area

---

Tue Jul 03 10:39:58 2007

### Data Source

Source Data File Name: D:\marcin\DSMs\XYZ\_data\abn.dat  
X Column: A  
Y Column: B  
Z Column: C

### Data Counts

Active Data: 2683991  
Original Data: 2840870  
Excluded Data: 0  
Deleted Duplicates: 156879  
Retained Duplicates: 155457  
Artificial Data: 0  
Superseded Data: 0

### Univariate Statistics

---

	X	Y	Z
Minimum:	6432995.401	5663233.936	93.683
25%-tile:	6433085.964	5663431.572	118.031
Median:	6433163.585	5663615.648	119.283
75%-tile:	6433225.903	5663784.491	134.34
Maximum:	6433300.2	5664045.126	165.437
Midrange:	6433147.8005	5663639.531	129.56
Range:	304.79900000058	811.19000000041	71.754
Interquartile Range:	139.93900000025	352.91900000069	16.309
Median Abs. Deviation:	68.012000000104	175.90000000037	1.676
Mean:	6433155.2247426	5663613.2918416	124.67675528272
Trim Mean (10%):	6433156.1709033	5663611.6933417	124.10034289966
Standard Deviation:	82.419130268283	210.44483205615	8.7432851624421
Variance:	6792.9130341802	44287.027339143	76.44503543178
Coef. of Variation:			0.070127628382818
Coef. of Skewness:			0.89777173828927

---

---

## Matching Data Statistics Report for MOP Area

---

Tue Jul 03 10:45:49 2007

### Data Source

Source Data File Name: D:\marcin\DSMs\XYZ\_data\mop.txt  
X Column: A  
Y Column: B  
Z Column: C

### Data Counts

Active Data: 2556293  
Original Data: 2567687  
Excluded Data: 0  
Deleted Duplicates: 11394  
Retained Duplicates: 11394  
Artificial Data: 0  
Superseded Data: 0

### Univariate Statistics

---

	X	Y	Z
Minimum:	6430040.4972	5665334.256	82.9246
25%-tile:	6430203.8379	5665434.3629	114.5796
Median:	6430406.6582	5665505.7889	115.2546
75%-tile:	6430608.0891	5665574.957	119.2964
Maximum:	6430874.2965	5665677.5206	143.9607
Midrange:	6430457.39685	5665505.8883	113.44265
Range:	833.79930000007	343.264600000034	61.0361
Interquartile Range:	404.251200000076	140.594100000034	4.7168
Median Abs. Deviation:	202.06149999984	70.164400000125	1.0279
Mean:	6430411.6770488	5665502.457619	117.89148148135
Trim Mean (10%):	6430409.0938656	5665502.7995351	117.39135968292
Standard Deviation:	226.51279707564	82.604501780891	5.4691720961927
Variance:	51308.047239028	6823.5037144693	29.911843417773
Coef. of Variation:			0.046391580014693
Coef. of Skewness:			1.4703753853808

---

---

## Grid Information for ABN area

---

Mon Jul 09 21:20:25 2007

Grid File Name: E:\Surfer\_grd\abn06\_cut\_med.grd  
Grid Size: 1354 rows x 509 columns  
Total Nodes: 689186  
Filled Nodes: 666564  
Blanked Nodes: 22622

### Grid Geometry

X Minimum: 6432995.4  
X Maximum: 6433300.2  
X Spacing: 0.599999999999963

Y Minimum: 5663233  
Y Maximum: 5664045  
Y Spacing: 0.60014781966001

### Grid Statistics

Z Minimum: 101.48361705074  
Z 25%-tile: 118.19122349389  
Z Median: 119.66532517033  
Z 75%-tile: 129.92031276832  
Z Maximum: 163.32658484229

Z Midrange: 132.40510094651  
Z Range: 61.842967791556  
Z Interquartile Range: 11.72908927443  
Z Median Abs. Deviation: 1.9903151644412

Z Mean: 124.17282733092  
Z Trim Mean (10%): 123.55687480132  
Z Standard Deviation: 8.1123924880748  
Z Variance: 65.810911880572

Z Coef. of Variation: 0.065331463110324  
Z Coef. of Skewness: 1.0768002606423

Z Root Mean Square: 124.43754240275  
Z Mean Square: 15484.701959236

---

## Grid Information for ABN area

---

Mon Jul 09 21:22:13 2007

Grid File Name: E:\Surfer\_grd\abn09\_cut\_med.grd  
Grid Size: 902 rows x 339 columns  
Total Nodes: 305778  
Filled Nodes: 296085  
Blanked Nodes: 9693

### Grid Geometry

X Minimum: 6432996.5978062  
X Maximum: 6433300.6124314  
X Spacing: 0.89945155393178

Y Minimum: 5663233  
Y Maximum: 5664045  
Y Spacing: 0.90122086570477

### Grid Statistics

Z Minimum: 103.24790628768  
Z 25%-tile: 118.19564346151  
Z Median: 119.6534888818  
Z 75%-tile: 129.89782787719  
Z Maximum: 162.70994161687

Z Midrange: 132.97892395228  
Z Range: 59.462035329191  
Z Interquartile Range: 11.702184415682  
Z Median Abs. Deviation: 1.9705687086557

Z Mean: 124.16871414068  
Z Trim Mean (10%): 123.55025837002  
Z Standard Deviation: 8.0949962115948  
Z Variance: 65.528963665734

Z Coef. of Variation: 0.065193525338624  
Z Coef. of Skewness: 1.0790210657575

Z Root Mean Square: 124.43230502975  
Z Mean Square: 15483.398535016

---

## Grid Information for MOP area

---

Mon Jul 09 09:44:07 2007

Grid File Name: E:\Surfer\_grd\mop06\_med.grd  
Grid Size: 573 rows x 1391 columns  
Total Nodes: 797043  
Filled Nodes: 797043  
Blanked Nodes: 0

### Grid Geometry

X Minimum: 6430040.497  
X Maximum: 6430874.297  
X Spacing: 0.59985611510778

Y Minimum: 5665334.256  
Y Maximum: 5665677.521  
Y Spacing: 0.60011363636305

### Grid Statistics

Z Minimum: 84.216296585421  
Z 25%-tile: 114.80519252295  
Z Median: 115.47707924953  
Z 75%-tile: 118.74603332811  
Z Maximum: 141.24027050053

Z Midrange: 112.72828354298  
Z Range: 57.023973915111  
Z Interquartile Range: 3.9408408051525  
Z Median Abs. Deviation: 1.2411552196866

Z Mean: 117.69255693933  
Z Trim Mean (10%): 117.21435342745  
Z Standard Deviation: 4.8417727775516  
Z Variance: 23.442763629439

Z Coef. of Variation: 0.041139158698433  
Z Coef. of Skewness: 1.6014532775443

Z Root Mean Square: 117.79210806564  
Z Mean Square: 13874.980722548

---

## Grid Information for MOP area

---

Mon Jul 09 21:23:54 2007

Grid File Name: E:\Surfer\_grd\mop09\_med.grd  
Grid Size: 382 rows x 927 columns  
Total Nodes: 354114  
Filled Nodes: 354114  
Blanked Nodes: 0

### Grid Geometry

X Minimum: 6430040.497  
X Maximum: 6430874.297  
X Spacing: 0.90043196544256

Y Minimum: 5665334.256  
Y Maximum: 5665677.521  
Y Spacing: 0.90095800524846

### Grid Statistics

Z Minimum: 84.795654679321  
Z 25%-tile: 114.81199472975  
Z Median: 115.47064966019  
Z 75%-tile: 118.72384722141  
Z Maximum: 140.96983064706

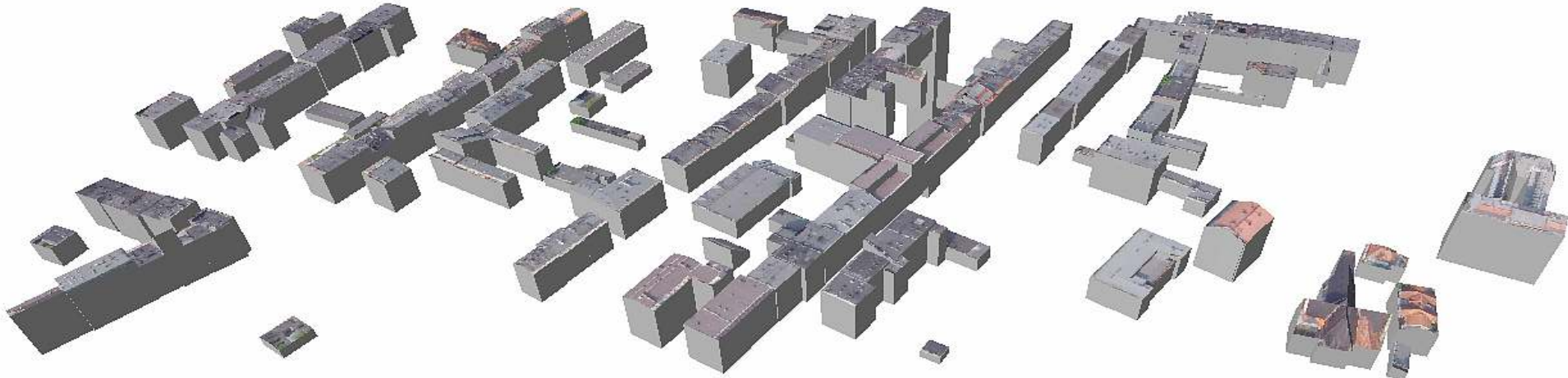
Z Midrange: 112.88274266319  
Z Range: 56.174175967741  
Z Interquartile Range: 3.9118524916592  
Z Median Abs. Deviation: 1.2240653067547

Z Mean: 117.68410551356  
Z Trim Mean (10%): 117.20508166944  
Z Standard Deviation: 4.8282341671908  
Z Variance: 23.311845173228

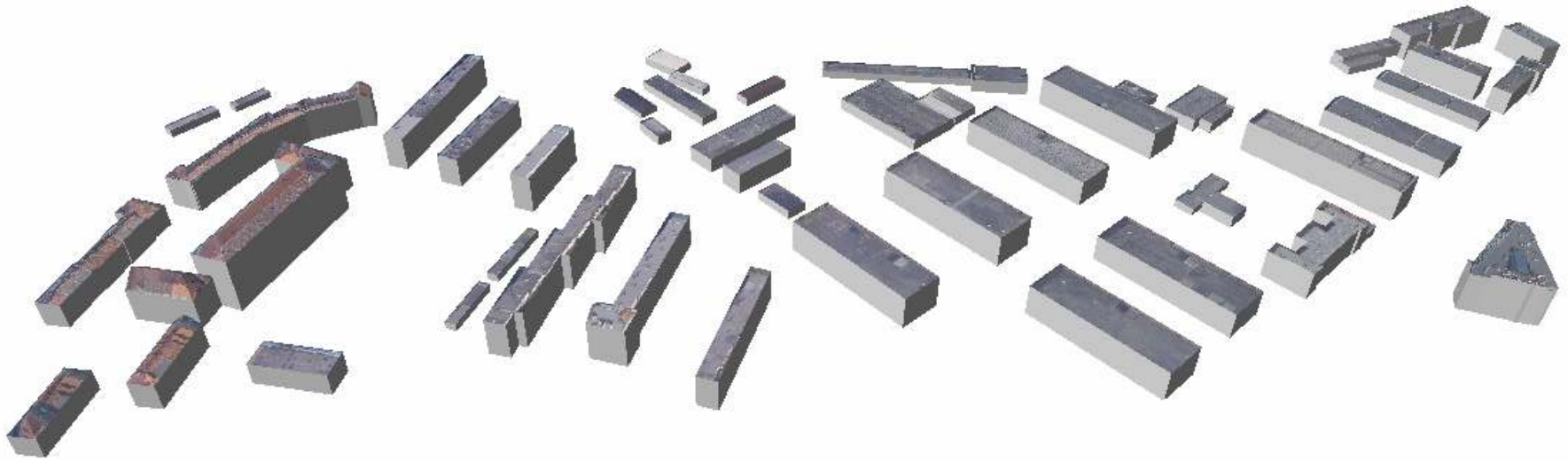
Z Coef. of Variation: 0.041027071125034  
Z Coef. of Skewness: 1.6081098830116

Z Root Mean Square: 117.78310802361  
Z Mean Square: 13872.8605357

**ABN area**



MOP area



## REFERENCES

- Ackerman, F. (1984): *High Precision Image Correlation*, 39th Photogrammetry Week, Stuttgart
- Ameri, B. and Fritsch, D. (2000): *Automatic 3D building reconstruction using plane-roof structures*, Proceedings of ASPRS, Washington DC
- Baillard, C. and Zisserman A.. (2000): *A plane-sweep strategy for the 3D reconstruction of buildings from multiple images*, 19th ISPRS Congress and Exhibition, Vol. 32, pp. 56-52
- Brenner, C. (2000): *Towards fully automatic generation of city models*, IAPRS, Vol XXXIII, Part B3 (Amsterdam), pp. 85–92
- Brenner, C. (2006): *Extraction and modelling*, International Summer School “Digital Recording and 3D Modeling”, Aghios Nikolaos, Crete, Greece
- Brenner, C. and Haala, N. (1998): *Fast Production of Virtual Reality City Models*, D. Fritsch, M. English & M. Sester, eds, ‘IAPRS’, Vol. 32/4, ISPRS Commission IV Symposium on GIS - Between Visions and Applications, Stuttgart, Germany, pp 77-84
- Fischer, A., Kolbe, T.H., Lang, F., Cremers, A.B., Foerstner, W., Plumer, L. and Steinhage, V. (1998): *Extracting buildings from aerial images using hierarchical aggregation in 2D and 3D*. Computer Vision and Image Understanding **72** 2, pp. 185–203
- Flamanc, D., Maillet, G., and Jibrini, H. (2003): *3d city models an operational approach using aerial images and cadastral maps*, ISPRS Archives, Vol. XXXIV, Part 3/W8, Munich
- Foerstner, W. (1999): *3D-City Models: Automatic and Semiautomatic Acquisition Methods*, In: Photogrammetric Week 99, Fritsch & Spiller (eds.), Stuttgart, Germany, pp. 291-303
- Früh, C. and Zakhor, A. (2001): *Fast 3D model generation in urban environments*. IEEE Conf. on Multisensor Fusion and Integration for Intelligent Systems, Baden-Baden, Germany, pp. 165-170
- Fuchs, C.; Gulch, E.; Forstner, W. (1998): *OEEPE Survey on 3D-City Models*, OEEPE Publication, No. 35, Bundesamt für Kartographie und Geodäsie, Frankfurt, 1998, pp. 9-124
- Gröger, G.; Kolbe, T. H., Drees, R., Kohlhaas, A., Müller, H., Knospe, F., Gruber, U., and Krause, U. (2004): *Das interoperable 3D-Stadtmodell der SIG 3D der GDI NRW*, Version 2, <http://www.ikg.uni-bonn.de/sig3d/>
- Gruen, A. (2001): *Cities from the Sky: Photogrammetric Modeling of CyberCity is Coming of Age*, Geoinformatics, Vol. 4, No. 10, pp. 30~33.
- Gruen, A., Baltsavias, E, and Henricsson (1997): *Automatic Extraction of Man-Made Objects from Aerial and Space Images (II)*. Birkhäuser Verlag, Basel, Ascona, Switzerland
- Jacobsen, K. (2005): *Photogrammetry and Geoinformation Trends for Large Scale Mapping*, Map Middle East. Dubai
- Jacobsen, K. (2006): *Digital surface models of city areas by very high resolution space imagery*, EARSeL Workshop on Urban Remote Sensing, Berlin,

Jibrini, H., Papanoditis, N., Deseilligny, M.P., Maitre, H. (2000): *Automatic building reconstruction from very high resolution aerial stereopairs using cadastral ground plans*. XIX'th ISPRS Congress, Amsterdam

Kada, M. (2003): *3D Building Generalization and Visualization*, Fritsch, Dieter (ed.): Proceedings of Photogrammetric Week '03, Stuttgart.

Kolbe, T. H., Gröger, G., Plümer, L.. (2005): *CityGML - Interoperable Access to 3D City Models*, van Oosterom, Peter, Zlatanova, Sisi, Fendel, E.M. (eds.): Geo-information for Disaster Management. Proceedings of the 1st International Symposium on Geo-information for Disaster Management, Delft

Kolbe, T.H. (2004): *Interoperable 3D-Visualisierung – 3D Web Map Server*, KS Band 9 - Der XFactor- Mehrwert für Geodaten und Karten, Bonn, pp. 130-140

Leberl, F., Gruber, M., Ponticelli, M., Bernögger, S., Perko, R. (2003): *The UltraCam Large Format Aerial Digital Camera System*, Proceedings Of The American Society For Photogrammetry & Remote Sensing Anchorage, Alaska

Reddy, M. (1998): *Specification and Evaluation of Level of Detail Selection Criteria*, Virtual Reality: Research, Development and Application, 3(2): pp.132-143

Rottensteiner, F. and Briese, C. (2002): *A new method for building extraction in urban areas from high-resolution LIDAR data*, International Archives of Photogrammetry and Remote Sensing and Spatial Information Sciences, Vol.34, Part 3A, pp.295-301

Schilcher, M., Guo, Z., Klaus, M., Roschlaub, R. (1998): *Semi Automatic Derivation of 3D-City-Models from existing 2D-Geoinformationssysteme*, Spatial Information Science and Technology SIST, Wuhan, China

Schulze-Horsel, M. (2007): *3D City Models: Data Generation and Applications*, GIS Development Asia Pacific, pp. 26-30

Schwalbe, E., H.-G. Maas and Seidel, F. (2005): *3D Building Model Generation from Airborne Laser Scanner Data Using 2D GIS Data and Orthogonal Point Cloud Projections*, Workshop "Laser scanning 2005". IAPRS, Enschede, The Netherlands

Suveg, I., Vosselman, G. (2004): *Reconstruction of 3D building models from aerial images and maps*, ISPRS Journal of Photogrammetry and Remote Sensing 58 (3-4): pp. 202-224

Taillandier, F. (2005): *Automatic Building Reconstruction from Cadastral Maps and Aerial Images*, CMRT05, ISPRS, Vienne, Autriche

Thiemann, F. (2004): *3D-Gebäude-Generalisierung*, Theorie 2003 - Kartographische Bausteine Band 26. Koch, W.-G. (Ed.), Dresden, pp. 52-58.

Thurgood, J.D., Gruber, M., Karner, K.. (2004): *Multi-ray Matching for Automated 3D Object Modeling*, ISPRS, Istanbul

Vosselman, G. and Dijkman, S. (2001): *3D Building Model Reconstruction from Point Clouds and Ground Plans*, International Archives of the Photogrammetry, Remote Sensing and Spatial Information Sciences, vol 34, part 3/W4, Annapolis, MA, USA, pp.37- 44